

2019

Analysis of Acoustic Emission Signals in Aluminum and Composite Structures

Duy Quang Tran
North Carolina Agricultural and Technical State University

Follow this and additional works at: <https://digital.library.ncat.edu/dissertations>

Recommended Citation

Tran, Duy Quang, "Analysis of Acoustic Emission Signals in Aluminum and Composite Structures" (2019). *Dissertations*. 148.
<https://digital.library.ncat.edu/dissertations/148>

This Dissertation is brought to you for free and open access by the Electronic Theses and Dissertations at Aggie Digital Collections and Scholarship. It has been accepted for inclusion in Dissertations by an authorized administrator of Aggie Digital Collections and Scholarship. For more information, please contact iyanna@ncat.edu.

Analysis of Acoustic Emission Signals in Aluminum and Composite Structures

Duy Quang Tran

North Carolina A&T State University

A dissertation submitted to the graduate faculty
in partial fulfillment of the requirements for the degree of

DOCTOR OF PHILOSOPHY

Department: Mechanical Engineering

Major: Mechanical Engineering

Major Professor: Dr. Mannur Sundaesan

Greensboro, North Carolina

2019

The Graduate College
North Carolina Agricultural and Technical State University

This is to certify that the Doctoral Dissertation of

Duy Quang Tran

has met the dissertation requirements of
North Carolina Agricultural and Technical State University

Greensboro, North Carolina
2019

Approved by:

Dr. Mannur Sundaresan
Major Professor

Dr. Jagannathan Sankar
Committee Member

Dr. Dhananjay Kumar
Committee Member

Dr. Vinayak Kabad
Committee Member

Dr. Fredrick Ferguson
Department Chair

Dr. Janis Oldham
Committee Member

Dr. Clay S. Gloster, Jr.
Interim Dean, The Graduate College

Biographical Sketch

Duy Tran was born on Aug 13, 1987 in Da Nang, Viet Nam. He received his Bachelor of Art in Science degree in Mathematics and Physics from the University of North Carolina in Greensboro (UNCG). In August 2013, Duy was admitted to the master program in the department of Mechanical Engineering at North Carolina Agricultural and Technical State University, and he got his Master of Science in 2016. He keeps continuing his PhD by performed research on “Analysis of Acoustic Emission Signals in Aluminum and Composite Structures.”

Dedication

I am dedicating this dissertation to my parents for their continual love and support throughout of my life, and to my wife for her patience and support while I was working on this dissertation.

Acknowledgments

I would like to thank Dr. Mannur Sundaresan for helping, guiding and supporting me for this research and the committee for serving in my thesis evaluation. I also thank ISM lab members, Dr. Letchuman Sripragash, Mr. Bonaventure Mills-Dadson, and Dr. Kassahun Asamene for helping me in this work.

Table of Contents

List of Figures	ix
List of Tables	xiii
Abstract	1
CHAPTER 1 Introduction.....	3
CHAPTER 2 Literature Review	6
2.1 Propagation of Acoustic Emission Related Stress Waves in Isotropic Plates	6
2.2 Acoustic Emission Signals from Different Damage Modes in Carbon/Epoxy Composite Materials	7
CHAPTER 3 Finite Element Model and Analysis	12
3.1 Introduction.....	12
3.2 Finite Element Model	14
3.3 Finite Element Analysis.....	17
3.4 Comparison with Available Experimental Results.....	28
CHAPTER 4 Acoustic Emission in Cross-ply Composite Specimens under Tension.....	33
4.1 Attenuation of Stress Waves in Composite Laminates.....	33
4.2 Composite Material Failure Modes and Related Acoustic Emission Signal Characteristics.....	35
4.3 Materials and Instrumentation	37
4.4 Experimental Results.....	39
4.4.1 Frequency content of acoustic emission events.....	41
4.5 Classification of Acoustic Emission Events Based on the Waveform and Frequency Content.....	50
4.5.1 Low and intermediate frequency events.....	51
4.5.2 High frequency events.....	52

4.6 Detecting the Formation of Clusters of Adjacent Fiber Breaks	54
CHAPTER 5 Summary and Discussion	66
5.1 Acoustic Emission Wave Propagation in Isotropic Plates.....	66
5.2 Different Damage Modes in Composite Materials and the Onset of Critical Damage ...	66
References.....	69

List of Figures

Figure 1. Finite element model.	15
Figure 2a. At the beginning of formation of microcrack.	16
Figure 2b. The state at the end of the formation of microcrack.....	16
Figure 2c. Time step function.	17
Figure 3. Position of symmetric Lamb waves and shear horizontal waves.	18
Figure 4. Comparison of strain waveform along the 90 degree and 45 degree direction.	19
Figure 5. Angular variation of amplitudes of So and SH modes at 300, 500, and 750 mm.	20
Figure 6. Ratio of peak amplitudes at various radii for SH mode vs So mode.	22
Figure 7. Strain waveforms along the 0 degree direction as they reach 300, 500, and 600 mm. .	23
Figure 8. The variation of the ratio of peak amplitude along x axis/peak amplitude along y axis, with distance.	24
Figure 8b. The variation of peak amplitude along x,y,z axis with distance.	24
Figure 9. Y displacement of the surface node at 300 mm along the y axis.	25
Figure 10. The z displacement of the surface node at 300 mm along the y axis.	26
Figure 11. The x, y, and z displacements due to the propagating AE wave along 45-degree direction, at different distances.	27
Figure 12. The peak amplitude of maximum shear strain at different locations along the 45- degree direction.....	28
Figure 13. (a) Sketch of the pulser position along the edge describing the distance and angle to the shear sensor array. (b) A photograph of experimental setup for the pulser simulated emissions.....	29

Figure 14a. A comparisons are shown for waveforms as observed by resonant sensor (a), commercial shear sensor (b) and devised shear sensor (c) along with their respective wavelet analysis, as originated due to pulser as an in-plane source.	30
Figure 14b. Waveforms at (a) 30, (b) 45 and (c) 60 degrees respectively due to pulser impulse applied.	31
Figure 15. (a) A photograph of the specimen with end fixture utilized for fatigue loading, (b) Sensor layout for the fatigue crack propagation tests.	31
Figure 16. Comparison of AE waveforms due to crack growth as observed by PZT wafer sensor and shear sensor along with their wavelet analysis where S_0 is of high magnitude.	32
Figure 17. Attenuation of S_0 mode.	34
Figure 18. Attenuation of A_0 mode.	34
Figure 19. The frequency response of the bonded piezoelectric sensor.	36
Figure 20. Composite test specimens and the positions of bonded sensors.	38
Figure 21. Arrangement used for creating impact damage.	39
Figure 22. Cumulative number of acoustic emission events for specimen without initial impact damage.	40
Figure 23. Cumulative number of acoustic emission events for specimen without initial impact damage.	41
Figure 24. Acoustic emission events classified based on dominant frequency content for specimen CN1 without initial damage.	43
Figure 25. Acoustic emission events classified based on dominant frequency content for specimen CP3 without initial damage.	44

Figure 26. Acoustic emission events classified based on dominant frequency content for specimen with low level of initial impact damage.....	44
Figure 27. Acoustic emission events classified based on dominant frequency content for specimen with high level of initial impact damage..	45
Figure 28. Waveform and corresponding wavelet diagrams for a representative high frequency AE signals from cross-ply specimens.....	45
Figure 29. Waveforms corresponding to successive acoustic emission events at 30% of ultimate stress for CN1..	47
Figure 30. Frequency content of successive acoustic emission events at 30% of ultimate stress for CN1.	48
Figure 31. Waveforms corresponding to successive acoustic emission events at 90% of ultimate stress for CN1..	49
Figure 32. Frequency content of successive acoustic emission events at 90% of ultimate stress for CN1.	50
Figure 33. Clusters of identical waveforms in undamaged specimen 1	56
Figure 34. Clusters of identical waveforms in undamaged specimen 2	57
Figure 35. Clusters of identical waveforms in specimen with low level impact damage.....	58
Figure 36. Clusters of identical waveforms in specimen with high level impact damage-CP3... ..	59
Figure 37. Cluster size, time to form and range of acoustic emission amplitudes within each cluster for CN1 specimen	60
Figure 38. Cluster size, time to form and range of acoustic emission amplitudes within each cluster for CN2 specimen.....	61

Figure 39. Cluster size, time to form and range of acoustic emission amplitudes within each cluster for with initial 2 impacts damage CP2 sensor 3. 62

Figure 40. Cluster size, time to form and range of acoustic emission amplitudes within each cluster for with initial 3 impacts damage CP3 sensor 4 63

List of Tables

Table 1 Estimated ranges of amplitudes and frequencies for the three failure modes	42
--	----

Abstract

Acoustic emission signal in aluminum plates and composite specimens are examined in this dissertation. The first part of the dissertation examines the symmetric lamb wave modes generated by the spontaneous appearance of a central microcrack in an aluminum plate. The detected acoustic emission amplitude of these waves with radial and angular position of the sensing location was analyzed using finite element analysis. An important aspect of this study is the detailed characterization of the shear horizontal mode of the Lamb wave that is generated by simulated crack growth. This analysis indicates that the amplitude of the shear horizontal mode remains larger than the fundamental symmetric mode generated by a simulated through-the-thickness crack at the center of the plate. Design of new sensors capable of efficiently isolating and detecting shear horizontal mode was examined. The final sensor configuration chosen was reasonably successful in the experiments that employed simulated acoustic emission sources launched into an aluminum plate using pulsing transducer excited by a triangular pulse. However, this sensor was not able provide clean signals for detecting crack growth related shear horizontal mode during a fatigue crack growth experiment.

The second part of the dissertation was on the development of structural health monitoring technique capable of assessing damage in composite structural elements. Acoustic emission signals generated during quasi-static loading of cross-ply tensile specimens were examined to relate each category of signal to the type of failure event and the failure mode. Based on the frequency content of the signal these signals were categorized. As reported by a number of researchers in the past, the critical damage that occurs before the catastrophic failure are the formation of clusters of multiple fiber breaks. Currently, such clusters of fiber breaks are identified after the specimen is unloaded, using scanning electron microscopy, or through

miniature tensile specimens loaded inside the chamber of a computed tomography instrument. In this study it is hypothesized that nearly identical acoustic emission waveforms are generated by clusters of fibers failing together near the final failure. Hence such signals may be useful for forewarning the impending failure. This hypothesis was examined for both undamaged specimens as well as specimens that were subjected to transverse impact. In both cases, rapid increase in the clusters of identical acoustic emission waveforms were seen and were successful in predicting impending failure. This technique needs to be validated through more extensive tests so that it can be scaled up to monitor real life structures such as primary structures of aerospace vehicles.

CHAPTER 1

Introduction

The objective of structural health monitoring is to detect and assess any potential damage to load carrying members of aircrafts, bridges, and other life critical components. Several methods are currently being proposed to provide the situation awareness regarding the safety of these structures. They include Lamb wave interrogation, distributed fiber optic strain sensing, monitoring the changes in vibration mode shapes and frequencies, and acoustic emission monitoring. Each of these techniques have their advantages and disadvantages. Acoustic emission technique relies on sensing and measuring the stress waves generated when microscopic levels of crack initiation or propagation. Acoustic emission technique has been extensively studied in the past and it is being applied to increasing number of engineering applications. There are a number of standards on the measurement and application of acoustic emission technique (AET) to engineering applications. In most situations, AET has been applied as a nondestructive evaluation tool in which the structural integrity is being evaluated before they are introduced into service or for periodically assessing the integrity at regular intervals of time as in pressure vessel qualification. In these settings, commercial acoustic emission sensors are viable. These sensors are coupled to the surface of the structure to sense the motion transverse to the surface. Most commercial AE sensors are sensitive to a combination of particle displacement, velocity, and acceleration.

AET has also been considered as a tool for structural health monitoring, with sensors integrated into the structures that are deployed. It should be noted that the traditional AE sensors are bulky and do not lend themselves for integration into structural elements. In these situations, piezoelectric wafers bonded to the surface of the structure or embedded in the structure would be

preferable. Such bonded sensors have been developed and evaluated in the recent past. They are shown to be effective in monitoring AE signals, as discussed in the literature review. The sensors measure the in-plane strain due to the wave motion. Hence, the sensitivity of these bonded sensors is closely related to in-plane motion while the traditional AE sensors measure out of plane motion. The difference in the responses of these two types of sensors to different modes and frequencies of AE signals have not been studied.

In addition, recently the shear horizontal component of AE signals from crack growth has been identified and experimentally verified. It was shown that the peak amplitude of shear horizontal wave was more than two times the amplitude of the symmetric Lamb wave mode, corresponding to a crack growth in an aluminum plate. The shear horizontal wave has the unique advantage of being unaffected by water or liquid borne acoustic as well as friction induced noise. Both of these types of noise can severely affect the false positives seen in AE signals. The probability of detection of the shear horizontal wave versus the more commonly studied Lamb wave modes have not been examined. For establishing the feasibility of success in SHM applications, it is necessary to quantify the signal amplitudes at various locations in structural elements corresponding to a microscopic crack growth. Numerical techniques such as finite difference and finite element technique have been used in the past studying wave propagation. The first part of the present study will be devoted to the finite element analysis of the different wave fields caused by a microscopic crack growth in an aluminum plate and two types of composite laminates. This knowledge is likely to be helpful in the analysis and classification of acoustic emission signals.

The second part of the study is devoted to developing quantitative methods of assessing impact damage to composite structures based on acoustic emission signals. The damage to

composite specimens subjected to impact damage is studied. Even undamaged composite structural members experience significant damage that steadily increases as the static load level is increased. The types of damages include matrix cracks, delaminations, and fiber breaks. Under transverse impact load, localized and much more severe delaminations, matrix cracks, and fiber breaks occur. The combination of these damages can reduce the strength often by 50% or more. In carbon/epoxy structures such as aircraft wings or fuselage, such impact damages are not detectable by visual inspection. Other inspection techniques are time consuming and expensive. AE can provide an efficient means of SHM solution for such damages.

In an earlier study on the damage development in composite specimens under quasi-static loading, groups of near identical waveforms were seen close to the final failure of the specimen. These waveform clusters were associated with clusters of adjacent fiber breaks which appear in CT scans of composite specimens. This observation provides a unique opportunity in which it would be possible to identify impact damage to composite materials which otherwise will be difficult to identify and track. Hence, by monitoring such groups of AE waveforms, it may be possible to recognize the point at which the damage growth is turning unstable and it may still be possible to avert catastrophic failure. Results from AE tests on composite specimens with various levels of impact damage will be presented.

CHAPTER 2

Literature Review

This study is concerned with the stress waves that accompany the formation and growth of cracks in structural materials in the form of plates. The first part of the dissertation is concerned with numerical and experimental investigation of stress wave generated by damage growth in isotropic plates that have constant thickness. The second part of the dissertation is devoted to developing an experimental method capable of providing advance warning of impending failure in composite aerospace structures that may have undergone unanticipated damage such as a caused by transverse impact caused by tool drop on the wing of an aircraft.

2.1 Propagation of Acoustic Emission Related Stress Waves in Isotropic Plates

During crack or damage growth, part of the strain energy is converted into stress waves usually termed as acoustic emission (AE) and propagate away from the crack surfaces. These propagating stress waves can be detected by suitably located acoustic emission sensors to detect and locate the propagating cracks and estimate their rate of growth. Acoustic emission monitoring technique is now a well-established technique in non-destructive evaluation and structural health monitoring [Miller et. al., 2005]. In plate like structures, the stress wave propagates in the form of guided waves, termed Lamb waves [Lamb 1917]. Depending on the source, a number of different modes and frequencies of Lamb wave are generated. The propagation characteristics of Lamb waves has been extensively studied both for isotropic and anisotropic materials such as composite laminates [Mindlin 1958, Auld, 1990, Graff 1991, Rose 1999]. A major application of these principles is in the structural health monitoring based on Lamb wave interrogation of plate like structures, in which Lamb wave generated and propagated in structures, and based on the modifications to the received signal, possible defects are

identified and characterized [Janapati et al., 2016]. There are also several experimental studies on the characterization of Lamb wave propagation in composite laminates. Including attenuation [Asamene et. al., 2015, Tran 2015], fretting generated AE [Asamene et. al., 2012], and real time neural system [Kirikera 2008]. One of the major impediments in the adoption of acoustic emission technique is the uncertainty introduced by several extraneous sources of acoustic emission signals. Signal processing techniques are not available to reliably identify and eliminate AE signals from such spurious sources. Most studies on acoustic emission focus on the symmetric and anti-symmetric Lamb wave modes that are generated by crack initiation and propagation. The presence of shear horizontal mode of guided wave was first studied experimentally and numerically quite recently [Rajendra et. al., 2010, Sundaresan et. al., 2011]. In these studies, the shear horizontal mode of propagation was found to have several advantages over the symmetric and anti-symmetric modes of Lamb waves, including larger amplitude and lesser dispersion.

2.2 Acoustic Emission Signals from Different Damage Modes in Carbon/Epoxy Composite Materials

Carbon/epoxy composite structural materials undergo widely distributed, complex damage and progressively increasing damage as these materials are subjected to increasing quasi-static tensile load. The damage progression in composite materials and the appearance of different failure modes as a function of static and fatigue load has been extensively studied in the past. Highsmith and Reifsnider, 1982 identified the characteristic damage state in carbon/epoxy laminates. The failure modes include matrix cracks, delaminations, and fiber fractures that progressively appear in different locations and continue to grow. Some of these failure modes have substantial effect on the strength and durability of composite components, while others are

considered non-critical. Jamison et al, 1984, provided a detailed account of appearance of different damage modes including transverse matrix cracks, axial matrix splits, delaminations, and fiber breaks, under tension-tension fatigue. In their observation, cluster sizes of 4 adjacent fiber breaks were observed. Damage to the zero-degree laminae begin as distributed single fiber breaks, often in the proximity of adjacent matrix crack in off-axis plies. In the case of monotonic tensile loading, the density of transverse cracks, axial matrix splits, and delaminations at the intersection of transverse and axial cracks are not likely to be as dense as in fatigue loaded specimen [Talreja and Singh, 2012]. In both monotonic and fatigue loading cases, as the stress level increases multiple adjacent fiber breaks or clusters of fiber breaks form. The moderate amount of matrix cracks and even lesser extent of delaminations seen under static load in cross ply laminates have zero or very little effect on the strength of these laminates [Reifsnider and Case , page 25]. Since the zero-degree laminae are supporting the major portion of the applied load, the damage to these laminae are likely to lead to the final fracture. While isolated fiber fractures starting to occur from relatively load levels do not precipitate structural failure, clusters of fibers breaking in rapid sequence have been to be a precursor the structural failure. Hence, identifying the formation of clusters of adjacent fiber breaks becomes critically important for structural health monitoring of life critical structures such as aircrafts which could experience unexpected adverse events such as impact damage. Numerous experimental observations suggest that this fiber damage progression in the formation of clusters of fiber breaks of increasing size. The spread of the damage from one fiber break into its neighborhood is likely to be determined by the fiber strength statistics, prevailing stress, local fiber packing and alignment, as well as the ability of the matrix and interface to contain the fiber damage. Jamison 1986, observed that four adjacent fiber breaks occurring close to the final failure. A similar observation was also made for

a specimen under flexural loading within a SEM chamber [Sundaresan 1988]. Recent X-ray computed tomography (CT) studies have provided valuable insight into the progressive growth of damage in carbon/epoxy composite samples subjected to tensile load. Scott et al, 2011 used high resolution computed tomography to study the fiber damage progression in miniature cross-ply composite specimens. Isolated individual fiber breaks as well as clusters of fiber breaks were observed to increase in number as the load was increased. The largest cluster of 14 adjacent fiber breaks was found in these miniature composite specimens at 94% of the ultimate load. Such clusters appeared in locations where there was no prior damage. Rosini et. al, 2019, carried out statistical measurement of local morphology of carbon epoxy composites using CT and found the local environment including fiber packing, fiber misorientation, and fiber strength distribution together may have a role to play in triggering the tensile failure of the composite specimen. Na et al., 2019, used CT to monitor the progression of fiber breaks in miniature unidirectional carbon/epoxy specimens subjected to quasi-static tensile loading and found clusters of fiber breaks the largest of which included 34 adjacent fiber breaks. Li, Lomov, and Yan 2015, observed damage progression using backlit images of plain weave glass/epoxy laminates statically loaded in tension while recording acoustic emission signals. The damage modes that were observed optically were transverse matrix cracks, longitudinal matrix cracks, and delaminations, that included formation of new cracks or delaminations and their progressive growth. They found that the number of acoustic emission signals agreed well with the formation and growth of observed matrix cracks and delaminations. The low amplitude low frequency AE events were found to be related to the observed number of matrix cracks and high amplitude low frequency events were found to be related to the number of delaminations. Ono and Gallego

2012, provides a literature review of acoustic emission studies related to monitoring damage in composite materials up to 2012.

The temporal properties of AE signals, including amplitude, energy, rise time, duration, are traditionally used to characterize the AE from damage in composites in the past. Sundaresan et. al., 1994, used acoustic emission monitoring to estimate the fatigue durability of composite femoral prosthesis. Nkrumah et. al., 2005, found that total AE energy during the proof tests were a good indicator of fatigue life of impact damaged woven glass-epoxy composite specimens. Crivelli et al., 2015, studied the occurrence of different failure modes in a specifically designed specimen with suitable loading sequence. Initially matrix cracks were promoted, and corresponding acoustic emission events were recorded. Subsequently the specimen was subjected to fatigue loading that promoted delamination. Acoustic emission signals that were recorded during the two segments were found to be successfully separated using an unsupervised neural network.

Baker et. al., 2015, examined transverse matrix cracks in four different laminate configurations. They found that the stress level at which the cracks form, their number, the dominant Lamb wave modes (S_0 or A_0) excited by the event, and the AE frequencies depended on the position of the 90-degree laminae in the stacking sequence. 90-degree laminae located in the interior gave rise to high frequency S_0 modes while in other laminates the 90-degree laminae located at the surface gave rise to low frequency A_0 modes. They also found that the cumulative AE energy correlated with the transverse crack density. Aggelis et al., 2012, examined the transverse matrix crack density. Cumulative AE events, and wave velocity in a carbon/epoxy laminate $[0_4/90_4]_s$ that promoted the formation of transverse matrix cracks and delaminations. AE sensors with a bandwidth of 50 kHz to 800 kHz was used. Acoustic emission, pulse velocity and

stress data during six loading steps of increasing amplitudes were recorded. Analysis of these results indicated that wave velocity for this laminate initially increased due to the formation of matrix cracks and delaminations that directed the stress wave to propagate essentially along the outer 0-degree laminae. Scholey et al., 2010, studied the acoustic emission wave propagation characteristics in a large quasi-isotropic carbon/epoxy laminate using sensors having bandwidth of 0 to 450 kHz. They found that matrix cracking was dominated by S_0 Lamb wave mode that had clear angular dependence and delamination events were dominated by A_0 mode and did not have angular dependence with respect to source and sensor. Mailllet et. al., 2015, found that inclusion of attenuation of acoustic emission signal was important in recognizing the damage mode in composite material. Dzenis 2001, used multi-parametric filtering to relate AE signals with the damage mechanism to the damage in graphite-epoxy laminates. Marec 2008, used wavelet analysis with multivariate filtering of AE signals to monitor damage in glass fiber/polyester laminates. McCrory 2015, compared the reliability of using unsupervised waveform clustering, artificial neural network and measured amplitude ratio in classifying AE signals. Mizutani 2000, compared data with generated waveforms to find relation between Lamb wave properties and fracture modes. Djabali et. Al., 2019, used computed tomography, digital image correlation, and acoustic emission to study the damage evolution in 36 ply, thick carbon/epoxy composite specimens subjected to bending fatigue. They were able to track the different failure modes as a function applied strain.

CHAPTER 3

Finite Element Model and Analysis

3.1 Introduction

Prosser et. al., 1994 and Gorman 1991a, and 1991b examined Lamb wave-based analysis for interpreting acoustic emission signals from thin isotropic plates. The equation governing wave propagation under small deformation in three dimensional solid in terms of displacement is given by:

$$(\lambda + \mu)\nabla(\nabla \cdot \mathbf{u}) + \mu\nabla^2\mathbf{u} + \rho\mathbf{f} = \rho \frac{\partial^2 \mathbf{u}}{\partial t^2} \quad (1)$$

λ and μ in the Eqn 1 are Lamé' constants, ∇ is del operator, ρ is the mass density and \mathbf{f} being the body force. Solution to the wave propagation equations show that three distinct types of stress waves propagate in isotropic solid media, namely, longitudinal waves, for which the particle displacements are along the direction of propagation, transverse waves or shear waves for which the direction of particle displacements are normal to the direction of propagation, The velocity for the mode waves are

$$C_p = \sqrt{\frac{\lambda + \mu}{\rho}} \text{ and } C_s = \sqrt{\frac{\mu}{\rho}} \quad (2)$$

respectively, where, E is Young's modulus, ν is Poisson's ratio and ω is the circular frequency. In thin plates because of multiple reflections from the top and bottom surface of plate and mode conversion, guided waves are generated. The propagation characteristics of guided waves has been studied in detail in the past and forms the basis of Lamb wave based structural health monitoring techniques, Acoustic emission events such as crack growth and different types of damages in composite generate complex Lamb wave modes. For the first part of this dissertation, the focus is on the wave propagation in isotropic material such as aluminum plates. Most

acoustic emission studies have assumed that the primary acoustic emission waves that are generated by events such as crack growth are the symmetric and antisymmetric plate wave. The reason for this situation is probably since conventional sensors are designed to detect normal surface displacements caused by these symmetric and antisymmetric waves. The results from the numerical analysis to be presented later will show that the shear horizontal waves turn out to be larger in amplitude and propagate longer distances without dispersion. But they are not detectable through conventional acoustic emission sensors.

Consider a plate parallel to the xy -plane, the displacement field for symmetric and anti-symmetric SH mode is given by

$$u_y(x, z, t) = [A \sin(qz) + B \cos(qz)]e^{(kx - \omega t)} \quad (3)$$

The displacement field is derived from a reduced form of Eqn 1. In Eqn 3, the constants A and B are arbitrary, whereas term q is defined as $q = \sqrt{\omega^2 / (C_s^2 - k^2)}$, with k being wavenumber of the mode. Additionally, the cutoff frequency, phase velocity and group velocity of SH modes can be derived as follows:

$$(fh)_n = \frac{nC_s}{2}, \quad C_{ps}(fh) = 2C_s \frac{fh}{\sqrt{4(fh)^2 - (nC_s)^2}} \quad \text{and} \quad C_{gs} = C_s \sqrt{1 - \frac{(n/2)^2}{(fh/C_s)^2}} \quad (4)$$

where, $n = 0, 2, 4, \dots$ represents symmetric SH modes and $n = 1, 3, 5, \dots$ being antisymmetric SH modes. It should be noted that when $n = 0$ the phase velocity and group velocity equal the bulk shear wave velocity, i.e. $C_{ps} = C_{gs} = C_s$, meaning the wave is dispersionless. However, it is not same for the cases when $n = 1, 2, 3, \dots$. Although SH mode overall is dispersive the fundamental mode SH_0 is dispersionless. Additionally, as stated by Mindlin and Yang 2006, unlike extensional and flexural waves, SH waves do not observe mode conversion upon reflection. Analytical solution to the acoustic emission related wave propagation problem becomes intractable due to the finite dimensions of the plate and multiple modes excited by events such as

crack growth. Finite element analysis of wave propagation provides a practical solution to the problem. However, this approach requires considerable computational resources for obtaining the solution.

3.2 Finite Element Model

In this analysis a 3 mm thick aluminium plate with 1000 mm x 1000 mm dimensions was modelled using explicit finite element analysis. The first objective was to compare the numerical predictions with the experimental results and to understand how to optimize the type and placement of sensors on a plate like structure to increase the probability of detection and the smallest crack extension. The second objective was to estimate the effect of microcrack induced stress waves on creating additional damage in the neighbourhood. The plate was divided into 0.5 x 0.5 x 0.25 mm elements along the x, y, and z directions. To reduce the computational effort, symmetry along the x and y directions as well as the xy mid-plane was taken advantage and only one eighth of the plate was modelled, as showed in figure 1. The analysis was performed in a 32-processor workstation as well as in 640 processor cluster. Each simulation ran from 3 to 5 days and resulted in output files whose size was greater than 7 terabytes.

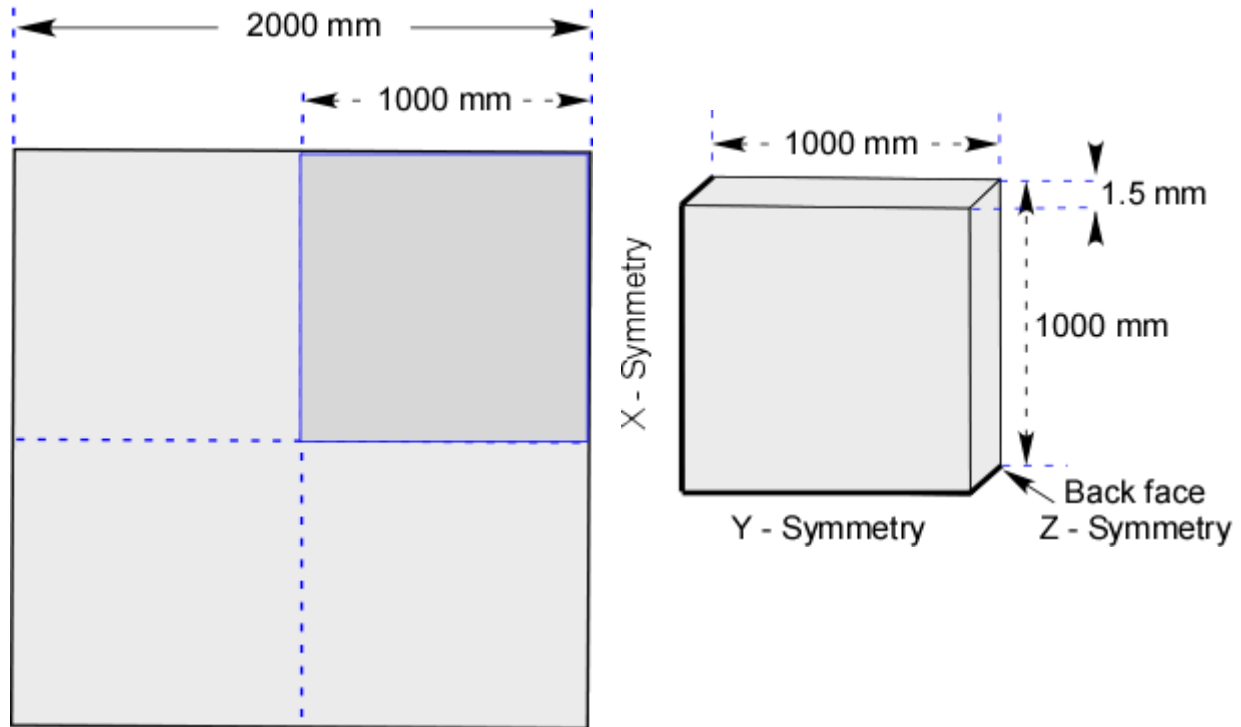


Figure 1. Finite element model.

The formation of a microcrack at the centre of this plate was simulated using the finite element analysis, using modified step function at the node at the centre. Figure 2 illustrated the superposition principle that used to show the equivalence between the release of stresses corresponding to a microcrack in a uniformly loaded plate and the step function applied at the central node in an unloaded plate, before the formation of microcrack. Figure 2(a) shows the superposition of uniform tensile load on the plate with an equivalent compressive load, resulting in a stress-free plate. Figure 2(b) shows the state at the end of the formation of microcrack. Here a uniform tensile load on the plate with centrally located microcrack is superposed with shows compressive load which results in a step function loaded on the crack surfaces. Assuming the microcrack is formed over 3 microseconds, the step function load at the crack surfaces will go from zero value to maximum value over a 3-microsecond duration, as showed in figure 2(c). The magnitude of the step function load was 100 Newton. This load was distributed uniformly across

the thickness of the plate, representing a centrally located through the thickness microcrack in the plate.

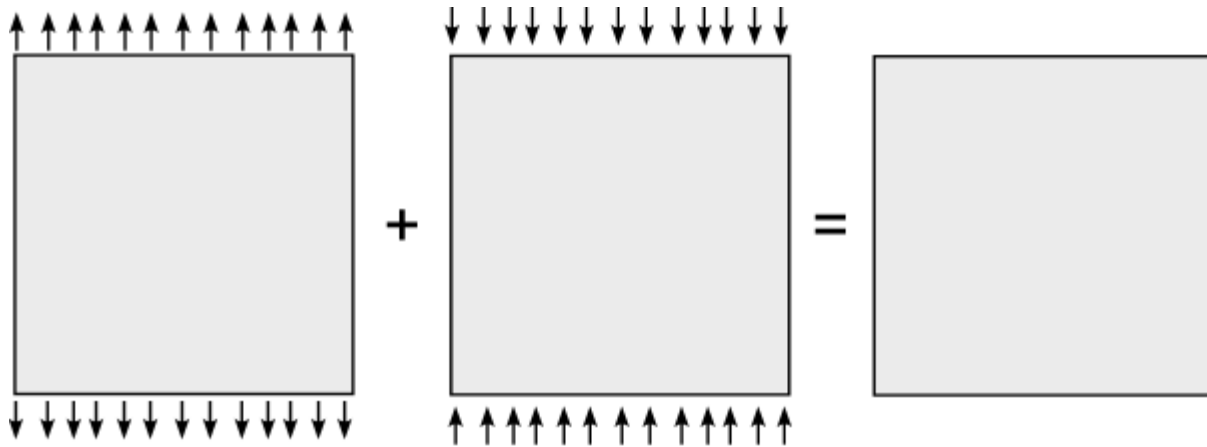


Figure 2a. At the beginning of formation of microcrack.

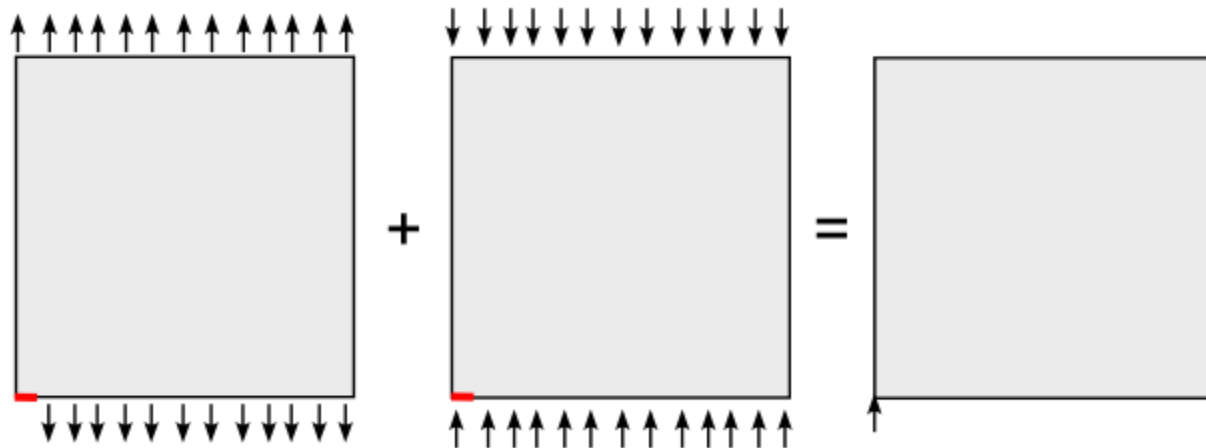


Figure 2b. The state at the end of the formation of microcrack.

As discussed by Moser [1], the accuracy of the result is determined by the temporal and spatial resolution of the simulation. The time step, Δt , used in the integration of this equation is important. Using a very short step size increases the computational time and very long time step, the higher frequency components are not resolved. It has been found that 20 points per cycle of the highest frequency of the stress wave being studied provides a good

compromise. Such a choice gives the relation $\Delta t = 1/f_{\max}$, where f_{\max} is the maximum frequency present in the signal. Since in the present investigation, the maximum frequency studied is 300 kHz, and a step size of 80 nanoseconds was used.

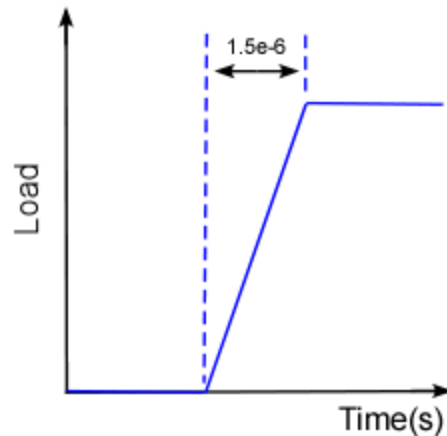


Figure 2c. Time step function.

For studying the stress waves, a 3-dimensional brick element with 8 nodes, with three degrees of freedom consisting of x , y , z displacements were used. Reduced integration was chosen to avoid shear locking phenomenon. The choice of the element size depends on the adequacy of the spatial resolution. Corresponding to the smaller velocity, namely, shear wave, and maximum frequency of 300 kHz, an element 0.5 mm long along the x and y direction, and 0.25 along the thickness direction was chosen. A 0.25 mm element size along the thickness direction was chosen to adequately represent the displacements along this direction. The number of elements needed for this computation was 2000 elements along x and y directions and 6 elements along the thickness direction. The large computational effort to solve this problem is clear from the mesh size and the time step involved.

3.3 Finite Element Analysis

The nature of propagating stress wave can be seen in the animations of wave propagation in the plate which are reproduced in figure 3. The instantaneous profiles of waves on the surface

of the plate at 300 microseconds and 500 microseconds are shown. The fringes corresponding to the S_0 mode as well those corresponding to shear horizontal component are shown.

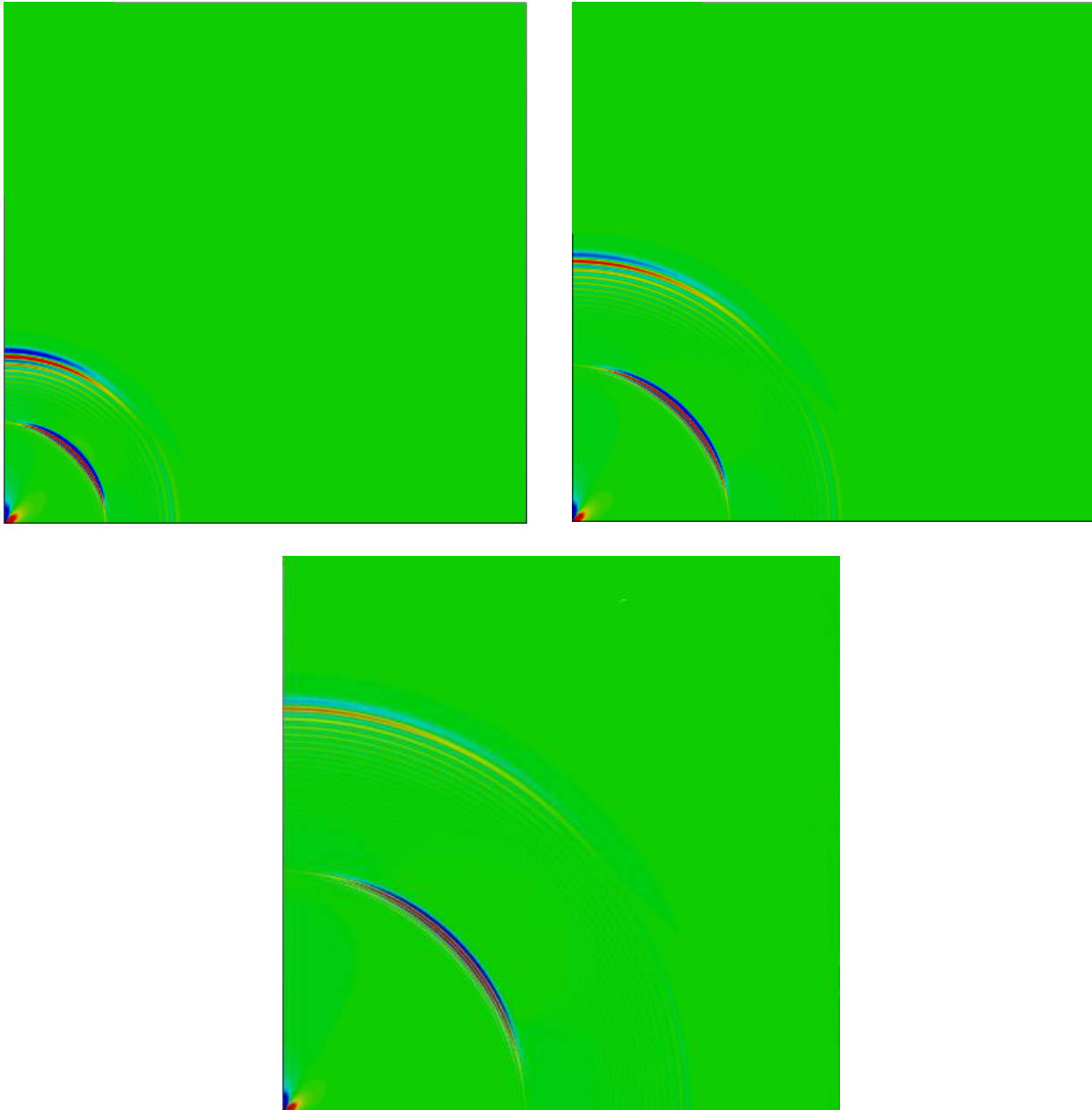


Figure 3. Positions of symmetric Lamb waves and shear horizontal waves at instances when the symmetric wave reaches 300, 500, and 700 mm.

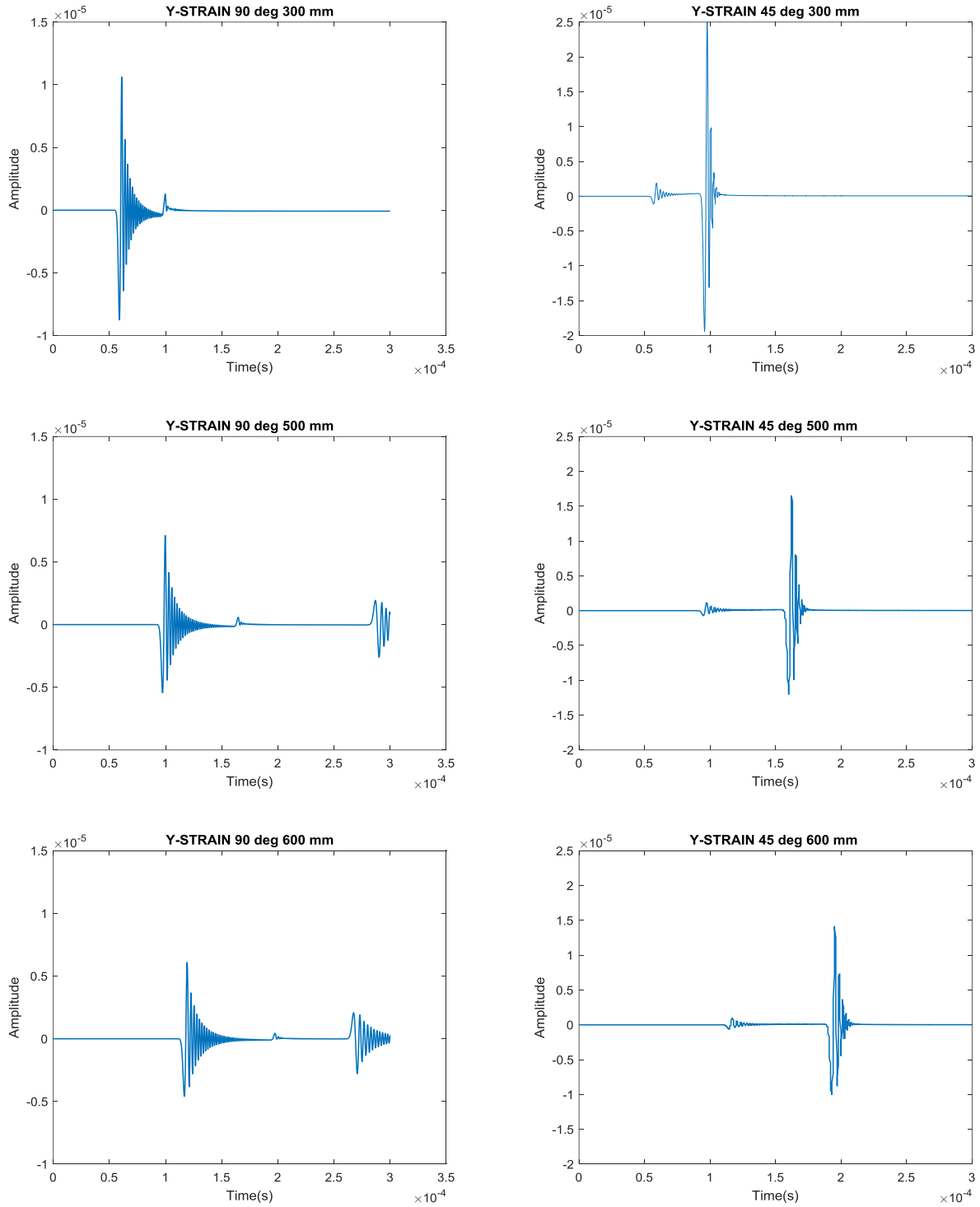


Figure 4. Comparison of strain waveform along the 90 degree direction (left) and 45 degree direction (right).

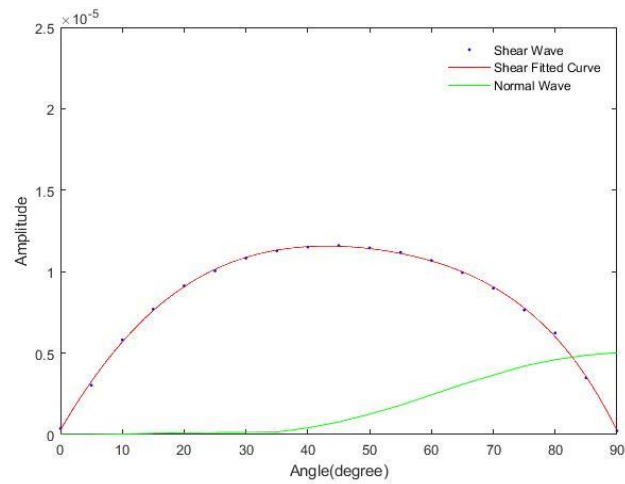
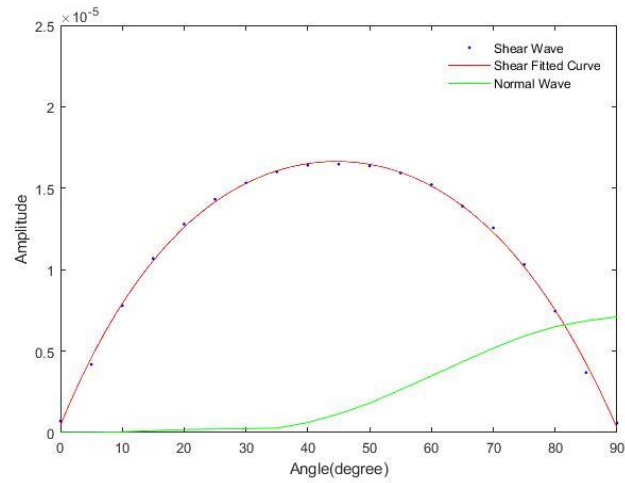
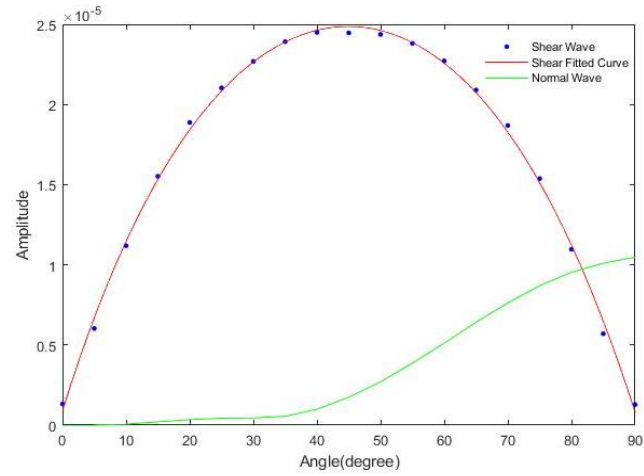


Figure 5. Angular variation of amplitudes of So and SH modes at 300, 500, and 750 mm.

These figures show that the symmetric lamb wave is dominant in the direction normal to the crack plane and its magnitude quickly decrease as the angle of propagation is moved away from 90 degrees. The shear horizontal wave is peaking at 45% with respect to the x axis and gradually decreasing as the angular position is decreased from this position.

Figure 4 compares the strain waveforms at 300, 500, and 700 mm along the y axis with waveforms along a line inclined at 45 degrees with respect to the y axis. In these figures the symmetric Lamb wave as well as shear wave components can be seen. The symmetric Lamb wave is much more dispersive compared to the shear wave component. The shear wave component seen along 45 degrees are substantially larger than the symmetric wave component seen along the y axis. The peak amplitudes of shear horizontal wave along the 45-degree direction are about 2.3 times peak amplitudes of So mode along the y-axis, and hence it is advantageous to devise sensors capable of detecting shear horizontal component of the acoustic emission signals. Figure 4 shows the angular variation of the peak values of So mode and shear horizontal mode with angles starting from 0-degree (i.e. in the x-direction) to 90-degree (i.e. y-direction). The peak amplitudes decrease with the radius. In addition, the peak amplitude of shear horizontal mode remains substantially higher than the peak value of the So mode for almost in all directions except very close to the 90-degree direction, indicating that the probability of detection of AE signal related to micro-crack formation based on shear horizontal component of the AE signal is many times greater than that of So component. Figure 5 shows the ratio of peak amplitudes of these two modes at the same radial distance, irrespective angle. Here the values seem to vary around 2.3 for all distances. The scatter seen at smaller radii is likely due to the position accuracy of 0.5 mm elements when the peaks at different directions are compared.

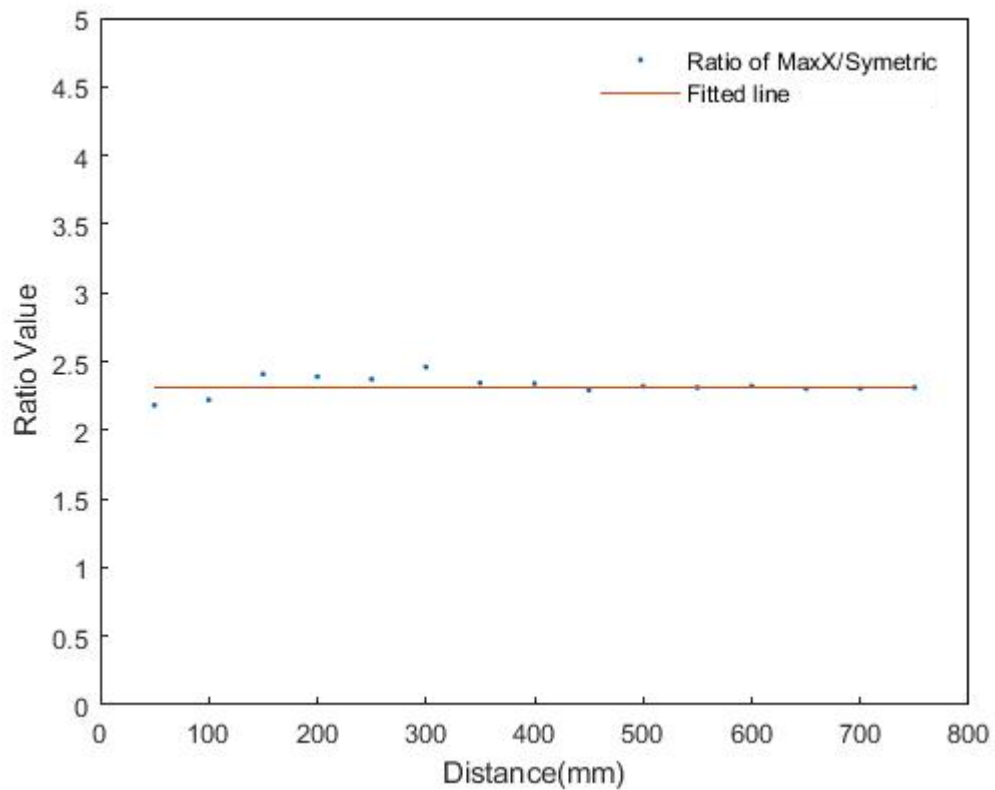


Figure 6. Ratio of peak amplitudes at various radii for SH mode vs So mode.

Figure 7 indicates the waveforms corresponding to y-strains at different distances along the x axis. The components corresponding to the shear horizontal wave appear to dominate the waveform. Figure 8 shows that the peak amplitude decays exponentially with distance from the crack tip. The important difference in the rate of amplitude reduction in the x direction compared to the other directions can be recognized.

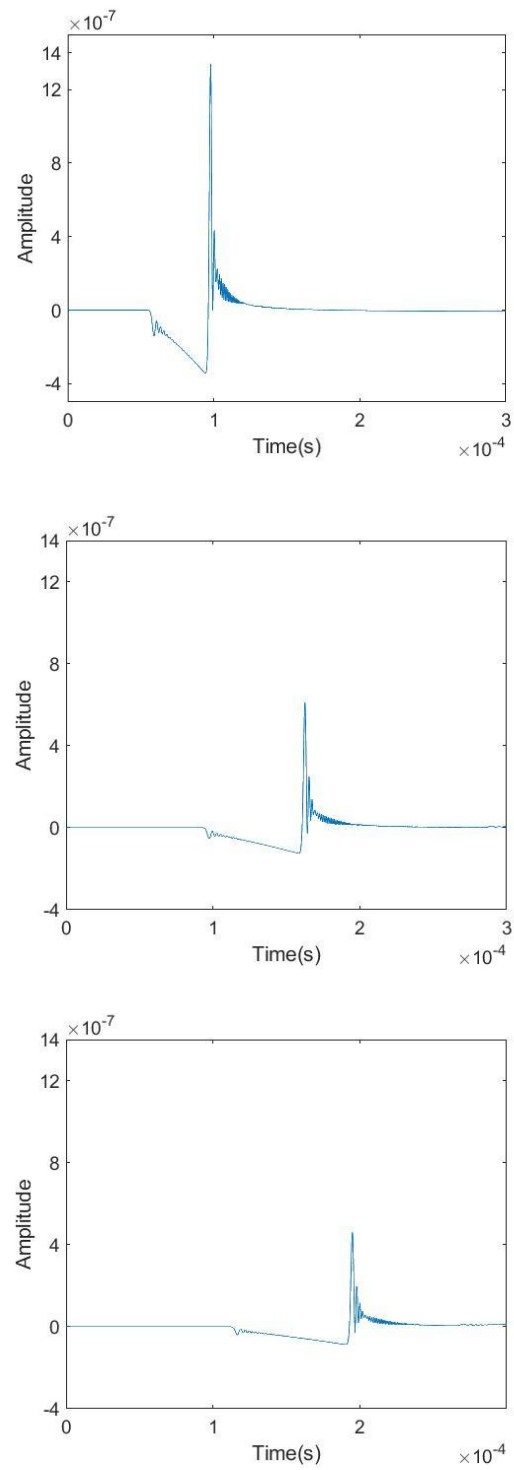


Figure 7. Strain waveforms along the 0 degree direction as they reach 300, 500, and 600 mm.

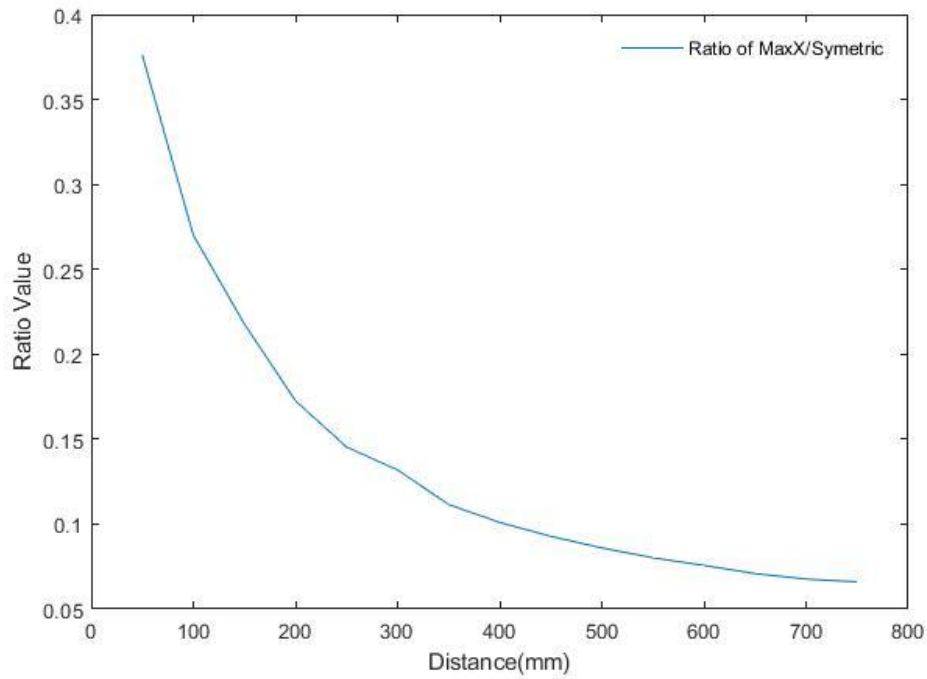


Figure 8. The variation of the ratio of peak amplitude along x axis/peak amplitude along y axis, with distance.

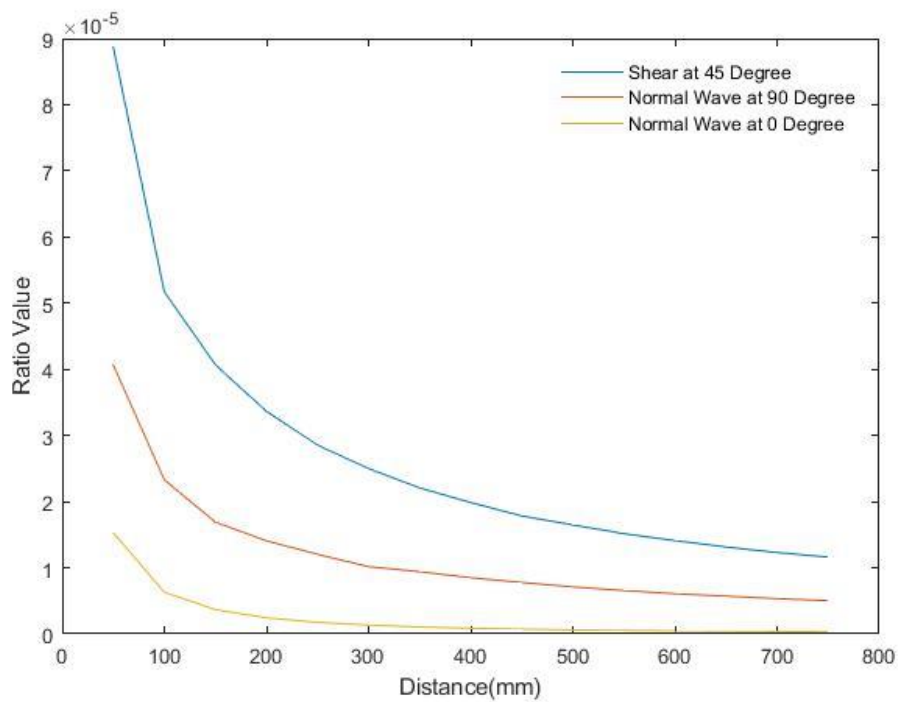


Figure 8b. The variation of peak amplitude along x,y,z axis with distance.

The x, y, and z displacements along different directions because of propagating wave are plotted in the following figures. It should be noted that traditional acoustic emission sensors detect AE signals from the z displacements at the surface. The bonded piezoelectric sensors detect AE signals from the in-plane strain, which in turn can depend on both the out of plane as well as in-plane displacements. The ratio of the displacements in y and z directions will affect the ratio of sensitivities of the bonded sensor vs conventional AE sensor. In this discussion only, symmetric Lamb wave is considered. Other considerations such as sensitivity to friction related noise may also be important. Figure 9 shows the y displacement of the surface node at 300 mm along the y direction. Figure 10 shows the z displacement for the same point.

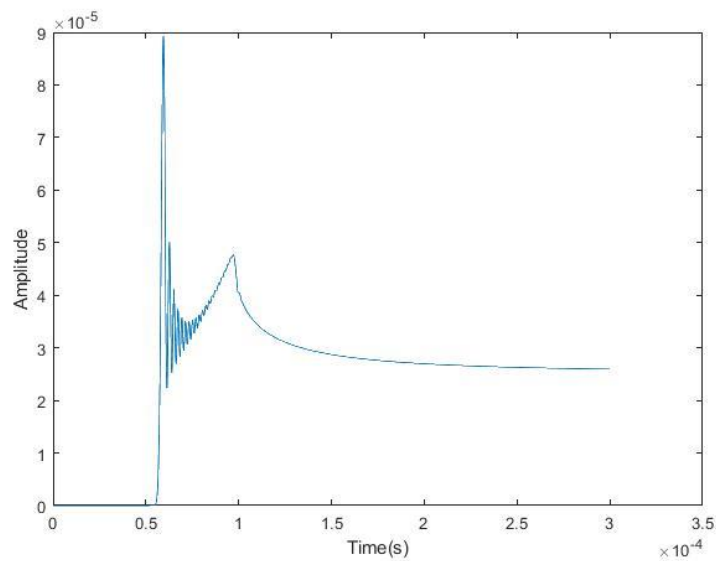


Figure 9. Y displacement of the surface node at 300 mm along the y axis.

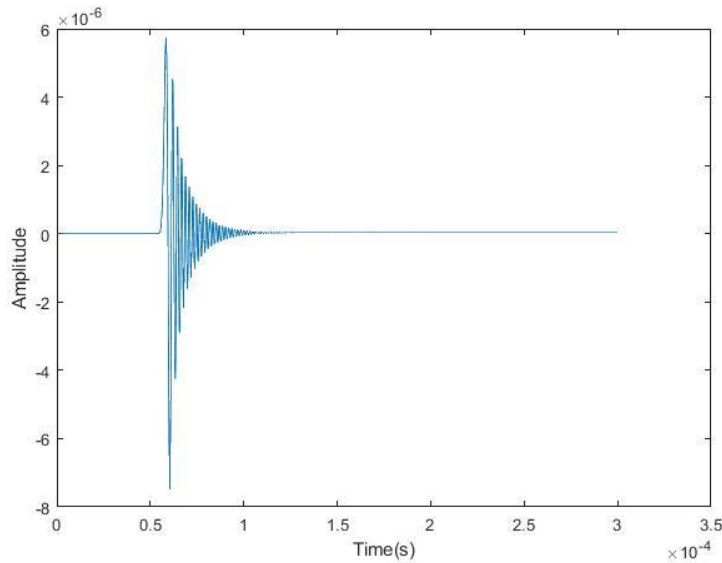


Figure 10. The z displacement of the surface node at 300 mm along the y axis.

The maximum shear strain due to the SH wave occurs along 45-degree direction and hence, the x , y , and z displacements and the maximum shear strain at various points along this direction is of interest from the sensing point of view. Figure 11 compares the magnitudes of x , y , and z displacements along the 45-degree direction in the plate. In x and y waveforms the displacements due to the arrival of shear horizontal mode is substantially larger than that of S_0 mode, by a factor of nearly 6. However, z waveform is exclusively due to the S_0 mode. Further, the peak amplitude of the z waveform is only about 15% of x and y waveforms. Figure 12 shows the maximum shear strain at different locations along the 45-degree direction. The peak values of the maximum shear strain, as expected, is due to the shear horizontal component.

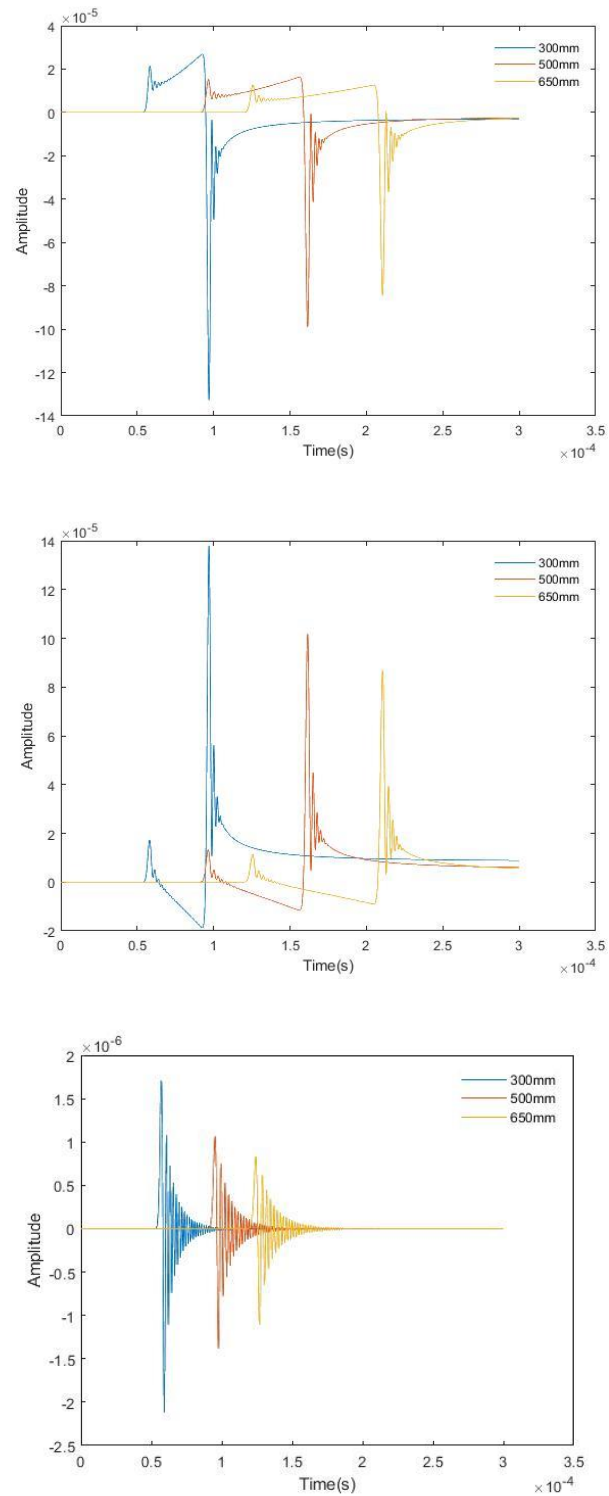


Figure 11. The x, y, and z displacements due to the propagating AE wave along 45-degree direction, at different distances.

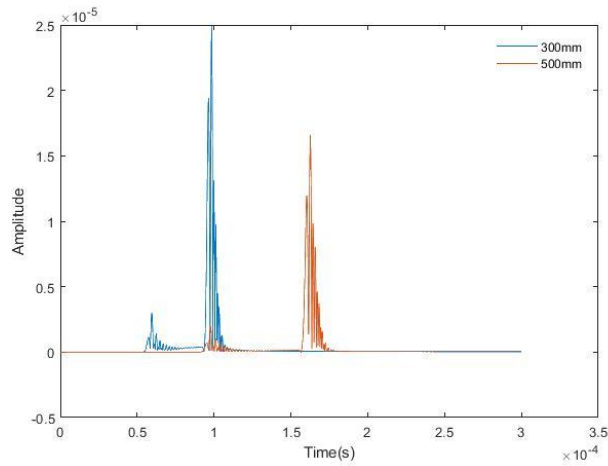


Figure 12. The peak amplitude of maximum shear strain at different locations along the 45-degree direction.

3.4 Comparison with Available Experimental Results

In this section, selected results of numerical simulations are compared with available results corresponding to the detection of shear horizontal waves studied by other investigators [Sundaresan et. Al., 2011, Supria 2012]. A sensor configuration shown in figure 13(a) was used to detect shear horizontal waves. Since this component of the wave attains its maximum value at an angular position of 45 degrees, the signal amplitudes at this position were measured. The simulated emissions were introduced by a piezoelectric transducer (SE650-P pulser) which was excited by a very short rectangular pulse. In addition, the transmitted stress waves were also detected by a commercial AE sensor (R30) and an ultrasonic shear wave sensor (V156). The experiment was setup as shown in Figure 13. A fixture was used to position the pulser along the edge of the specimen, which had been sanded, cleaned, and coated with petroleum jelly to ensure effective transmission of the impulse. The pulser excitation was set to 400V and the fixture

ensured application of the impulse at the mid-plane of the specimen. The waveforms were recorded at a sampling rate of 20 MHz.

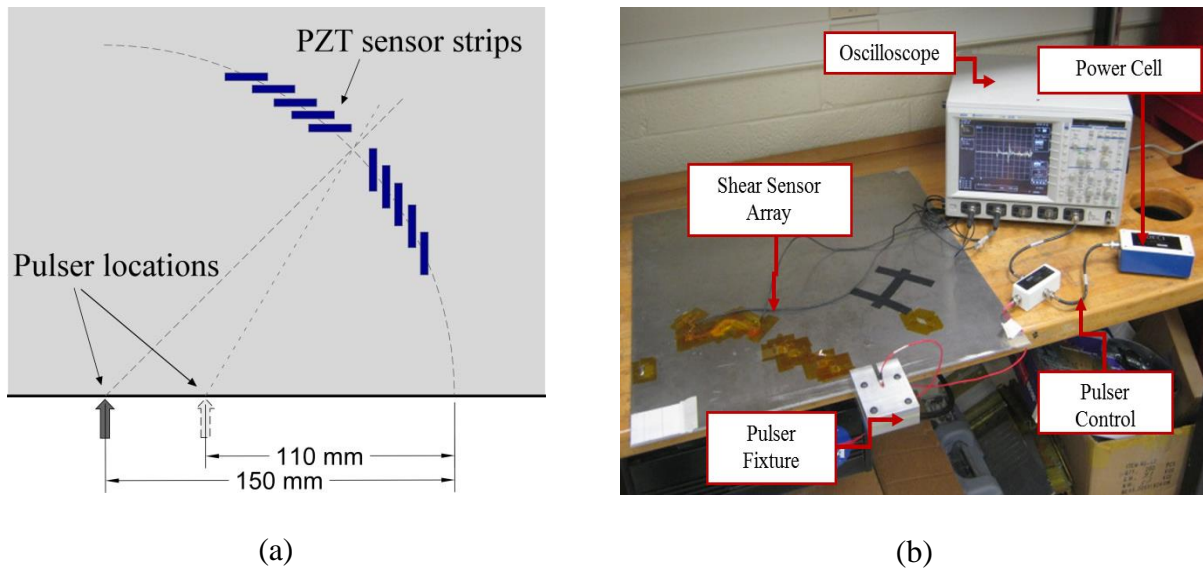


Figure 13. (a) Sketch of the pulser position along the edge describing the distance and angle to the shear sensor array. (b) A photograph of experimental setup for the pulser simulated emissions.

A comparison of the response of the three sensors to the simulated AE events are shown in Figure 14a. The commercial sensor (R30) response consisted of primarily 300 kHz signals. The ultrasonic shear wave sensor V156 and the bonded shear sensor both indicated distinct components corresponding to shear horizontal component. The relative magnitudes of the S_0 mode and the shear horizontal component as measured by the new shear sensor at different angular positions are compared in figure 14b. In these figures, the magnitude of shear horizontal wave relative to the S_0 component attains its peak at 45-degree angular position. These results are similar to the results from numerical simulations discussed earlier.

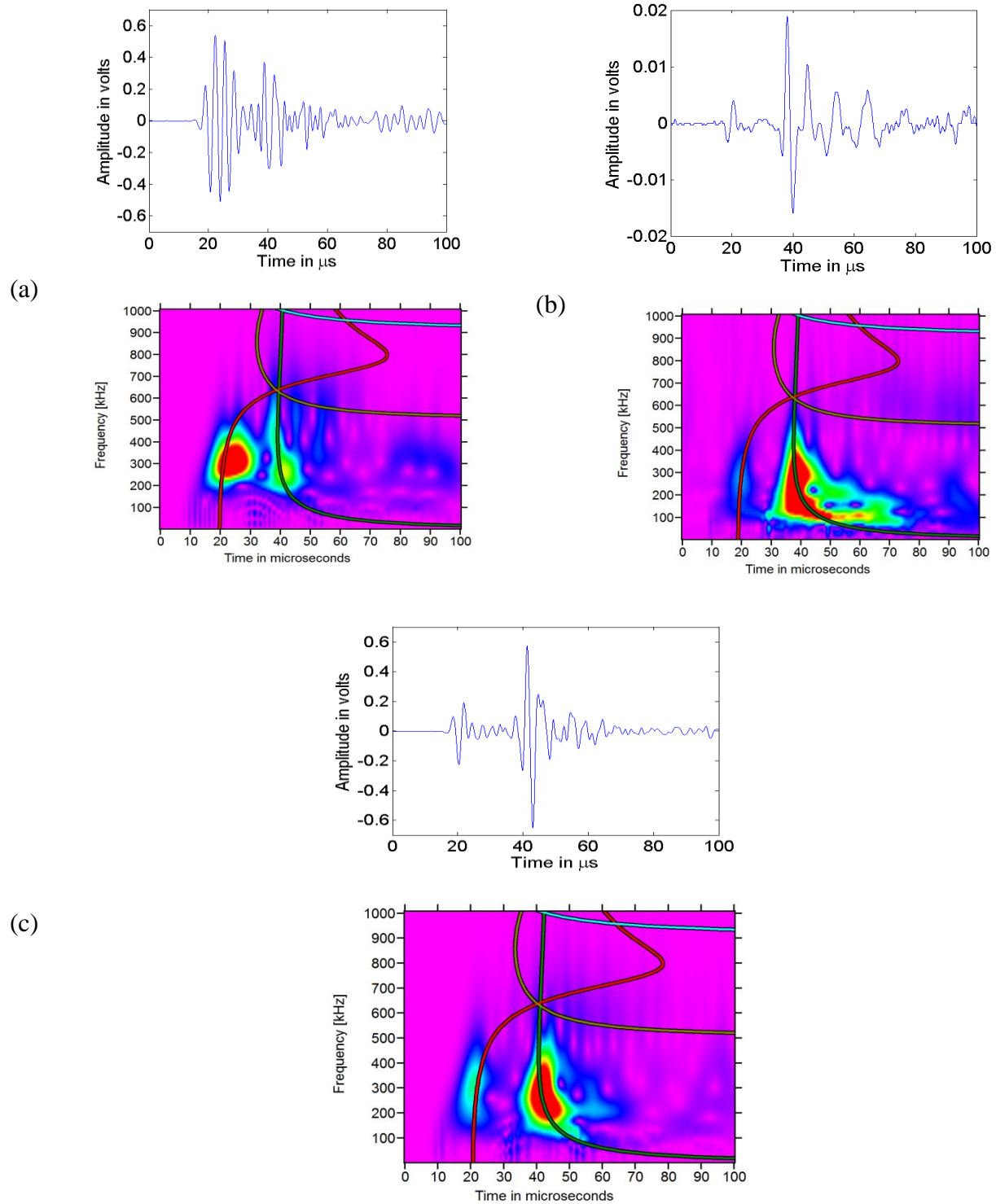


Figure 14a. A comparison of waveforms from resonant sensor (a), commercial shear sensor (b) and devised shear sensor (c) and their wavelets.

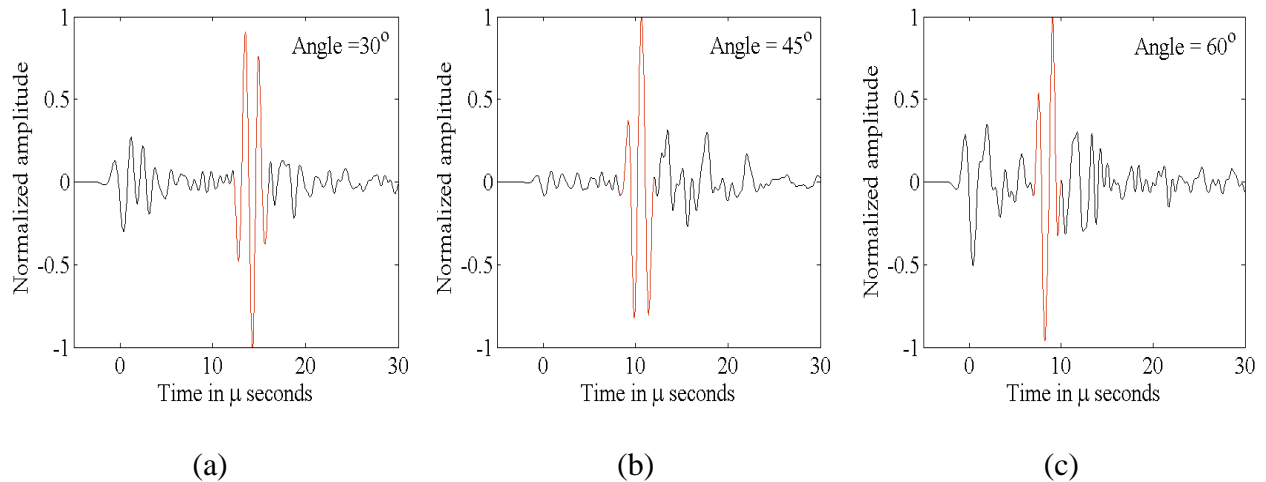


Figure 14b. Waveforms at (a) 30, (b) 45 and (c) 60 degrees respectively due to pulser impulse applied.

Acoustic emission signals from fatigue crack growth [31] is examined next. The experimental setup used in collecting these signals are shown in figure 15. The waveforms from regular piezoelectric wafer sensor along with the waveform from shear wave sensor is shown in figure 16. The presence of shear horizontal component in the waveform is evident.

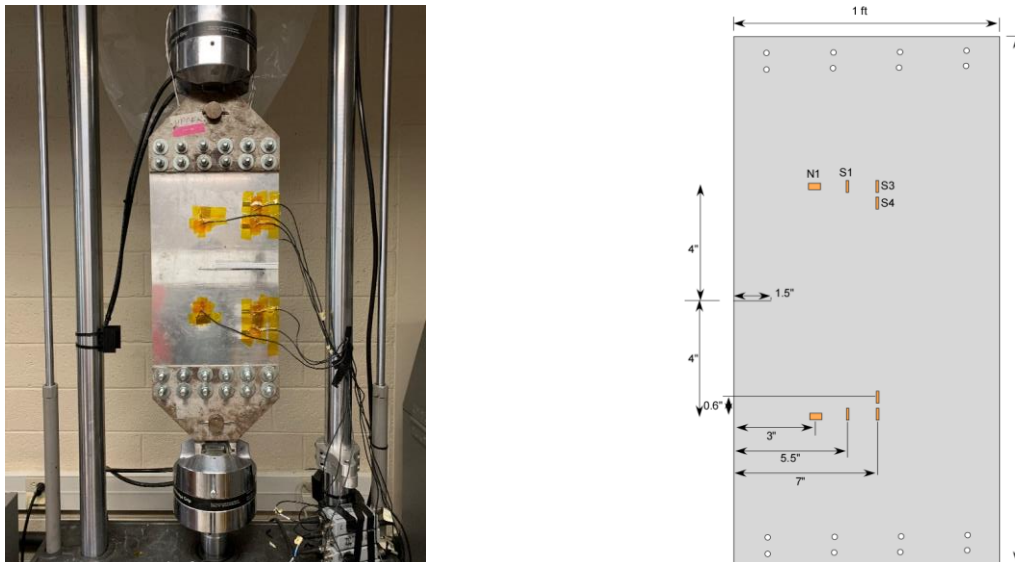
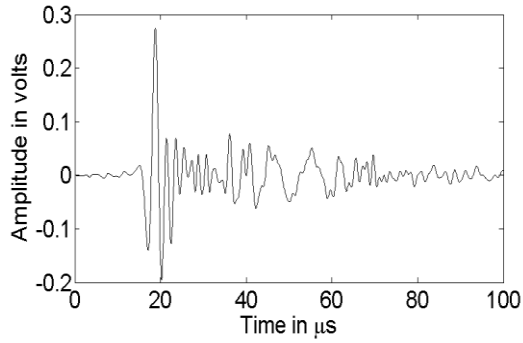
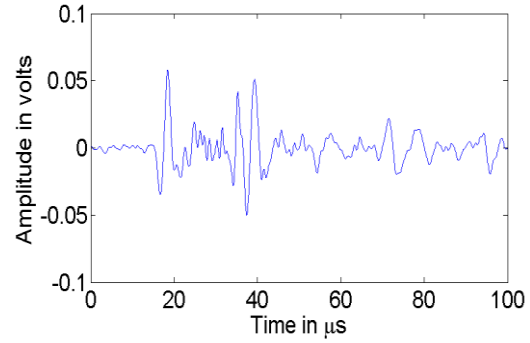


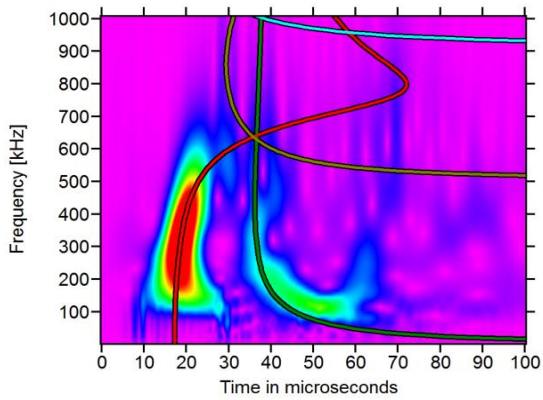
Figure 15. (a) A photograph of the specimen with end fixture utilized for fatigue loading, (b) Sensor layout for the fatigue crack propagation tests.



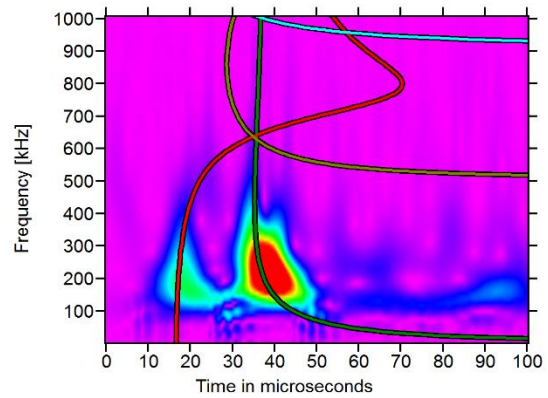
(a) AE signal from wafer sensor



(b) AE signal from devised shear sensor



(c) Wavelet analysis of the signal in (a)



(d) Wavelet analysis of the signal in (b)

Figure 16. Comparison of AE waveforms due to crack growth as observed by PZT wafer sensor and shear sensor along with their wavelet analysis where S_0 is of high magnitude.

CHAPTER 4

Acoustic Emission in Cross-ply Composite Specimens Under Tension

4.1 Attenuation of Stress Waves in Composite Laminates

Asamene et. al. 2015, and Tran 2015, experimentally determined the levels of attenuation in A_0 and S_0 Lamb wave modes in composite materials as a function of frequency up to a frequency of 400 kHz for A_0 mode and 500 kHz for S_0 mode. Since the attenuation levels increased rapidly beyond 500 kHz, it was not feasible to reliably measure the attenuation at higher frequencies. Experimentally determined attenuation of S_0 and A_0 modes of Lamb wave signals in cross-ply laminate along the 0-degree direction is shown in Figure 18. Attenuation was found to dramatically change AE waveforms and nearly eliminate these high frequency components even at distances of 50 to 100 mm from the source even when the frequency content was confined to 500 kHz. In the present experimental work acoustic emission signals extending to 2 MHz are observed. Based on the trend in the attenuation seen in figure 18, the sources of those signals are likely to be within about 10 or 15 mm from the source. Further, the attenuation levels shown in this figure is for cross-ply specimen without any damage. As cross-ply laminates are loaded, they undergo extensive and increasing distributed damage due to transverse cracks in 90-degree laminae as well as limited delaminations between 0-degree laminae and 90-degree laminae. This damage will reduce the region around each sensor from which high frequency signals will be able to reach the sensors.

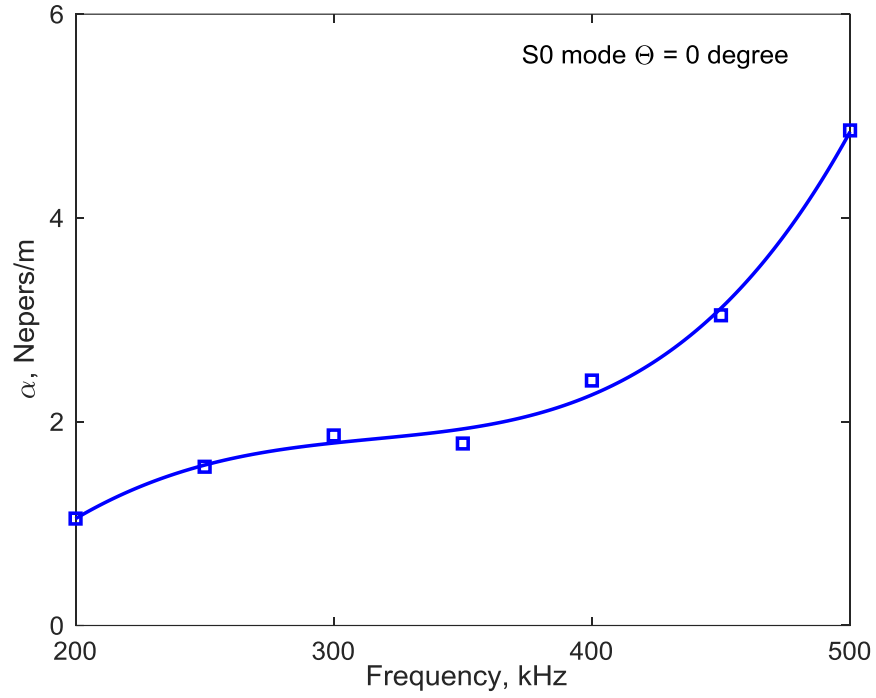


Figure 17. Attenuation of S_0 mode of in cross-ply laminates in the 0-degree direction.

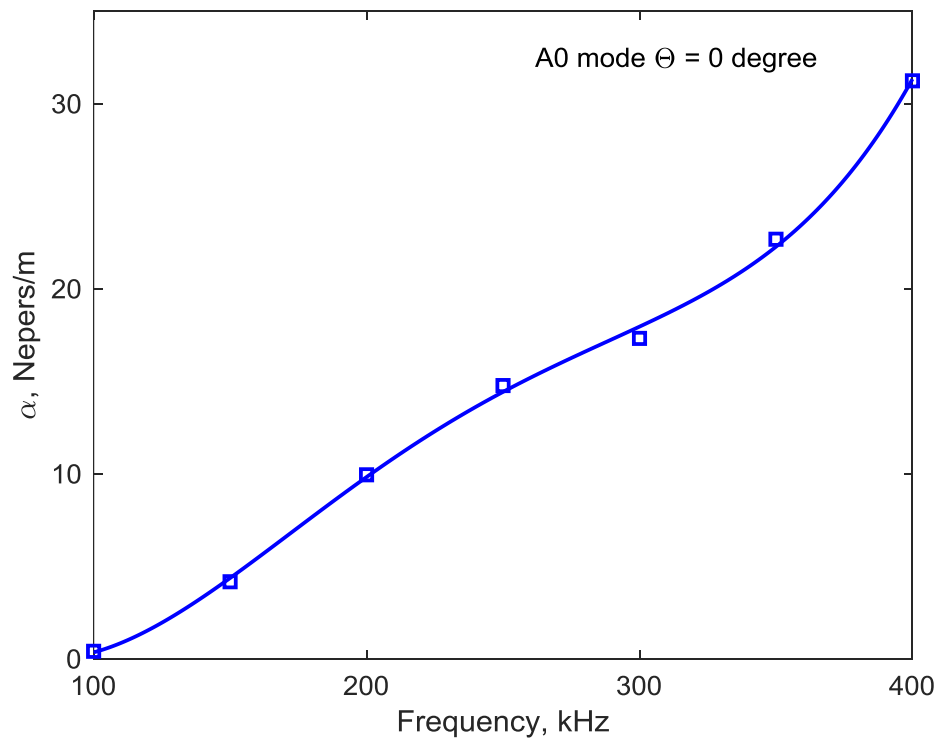


Figure 18. Attenuation of A_0 mode in cross-ply laminates in the 0-degree direction.

4.2 Composite Material Failure Modes and Related Acoustic Emission Signal

Characteristics

Although acoustic emission technique has been used to monitor damage growth in composite material for a long time, there is little consensus on successful use of AE signals to differentiate failure modes based on the AE parameters received from those failure events. Some of the factors that are responsible for the lack of correlation between AE and failure modes include the limited frequency bandwidth of available AE sensors, and the high attenuation seen in AE signals particularly in the frequency range likely to be associated with fiber fractures. In addition, if a failure event in each location may start as one failure mode and may transition into a different failure mode, but the acoustic emission waveform from this event will be influenced by both modes. The Lamb wave modes and frequencies generated depend on the duration of the failure, the failure mode in terms of if the impulse travels along the length of specimen as in fiber fractures and transverse matrix cracks or if the impulse causes a moment as in mode I or mode II delamination, and the position of the event relative to the midplane of the sensor. Fiber fractures and transverse matrix cracks are likely to result in mainly symmetric Lamb wave modes along with some antisymmetric components depending on failure location relative to the neutral axis. Delaminations are likely to result in predominantly antisymmetric Lamb wave modes. Since the frequency of propagation is limited by attenuation beyond 1 MHz, higher Lamb wave modes are not likely to be present. Even among those frequency components that are sensed, the lower frequencies below 300 kHz are likely to be detected even if the source to sensor distance is in of the order of 100 mm. However, frequencies greater than 500 kHz are likely to be detected only if the source to sensor distance is smaller than 50 mm. Hence in instrumenting the composite members and associating waveforms with source types, both the frequency content at the source

as well as modifications introduced by the medium during its transit must be taken into consideration.

Fiber failures in composite materials are likely to be very short duration events, because of the small cross-sectional area and high crack velocity associated with large stress with such breaks. Hence acoustic emission signals from fiber breaks are likely to have high frequency content compared to matrix cracks and delaminations. To be able to differentiate fiber breaks from other failure modes, sensors are required to have high fidelity as well as adequate bandwidth. Traditional acoustic emission sensors are limited by the “aperture effect” since acoustic emission waves travel parallel to the sensor surface when mounted on composite laminates, and the waves are not normally incident on the sensor face. Bonded piezoelectric wafers have been used for monitoring damage in composite laminates as well as metallic specimens [Whitlow 2013, Asamene 2012]. Jacques 2008, showed that bonded sensors can detect AE signals with high fidelity by comparing these signals with signals from a Laser interferometer.

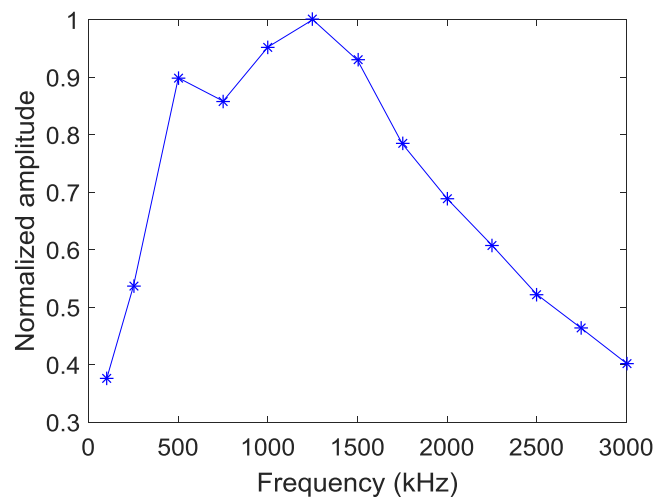


Figure 19. The frequency response of the bonded piezoelectric sensor, Mills-Dadson 2015.

These bonded piezoelectric sensors have been modified in the recent past to have an effective aperture width of 1 mm and having bandwidth in excess of 2 MHz. The frequency response of the bonded piezoelectric sensor is shown in Figure 19.

Whitlow 2013 used bonded AE sensors which were sensitive to frequency components up to 700 kHz and monitored damage progression in composite specimens and was able to associate AE events with the formation of multiple adjacent fiber breaks, based on correlation analysis. Such events were found to form within the last 5 to 10% of the ultimate load. Mills-Dadson 2015 used sensors whose sensitivity extended beyond 2MHz and examined AE waveforms from multidirectional composite specimens and tentatively associated low, mid, and high frequency events with delaminations, matrix cracks, and fiber breaks. As a part of this study new AE sensors capable of measuring frequencies to 2 MHz were developed. In addition, composite specimens were instrumented with sufficient number of sensors to capture high frequency signals before they are attenuated.

4.3 Materials and Instrumentation

Cross-ply carbon/epoxy tensile test specimens were prepared in accordance with ASTM Standard D3039. The stacking sequence was $[0/90]_{3s}$ and the specimens' dimensions were 300 mm \times 25 mm \times 1.8 mm, as shown in Figure 20. Two groups of specimens were instrumented and tested. The first group of specimens were normal test specimens without any initial damage. The other group of specimens were subjected to three different levels impact damage. These specimens were subjected to impact of a 10 mm diameter steel spherical indenter. The arrangement for subjecting the specimen to impact is shown in Figure 21. The specimen was held in between two steel plates with 10 mm diameter holes and 10 mm steel sphere was placed above the composite specimen at the impact site. A steel guide pipe was used to drop 150 gm

steel cylinder on to the steel sphere as indicated in Figure 21. Three levels of damage were introduced by repeating the impact 1, 2, or 3 times. Fiber glass tabs were bonded to both ends of each specimen for effective load transfer from the grips to specimen without damaging the specimen. On undamaged specimen, four rectangular piezoelectric (PZT) wafers with steel electrodes were bonded as shown in Figure 20. For the impact damaged specimens two acoustic emission sensors were bonded at 25 mm on either side of the impact damage. The signals from the transducers were amplified by 40 dB using commercial preamplifiers with 50 kHz high pass filters. For most specimens 40 dB threshold was set for acquiring the AE signals. The signals from the four channels were recorded by an acoustic emission monitoring system. In addition to the standard AE parameters for each of the events, waveforms were also recorded. Sampling rate of 20 million samples per second was used to acquire the waveforms. The specimens were loaded to failure in a servo hydraulic testing machine at a loading rate of 10 lbs/sec.

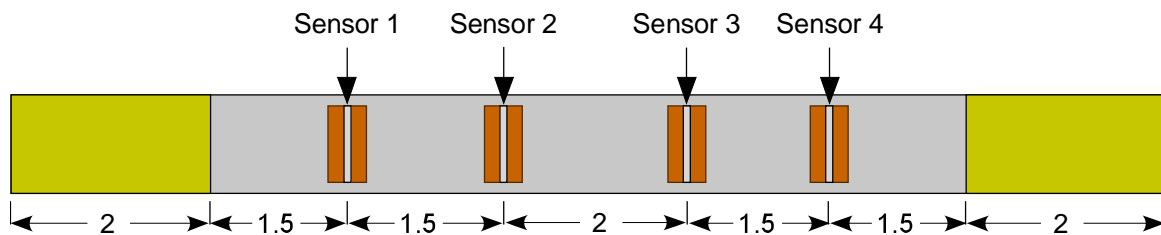


Figure 20. Composite test specimens and the positions of bonded sensors.

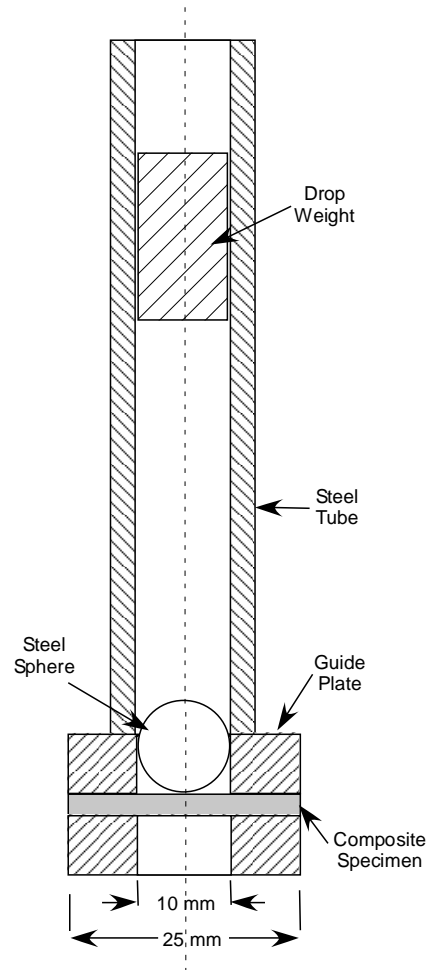


Figure 21. Arrangement used for creating impact damage.

4.4 Experimental Results

The average strength of undamaged cross-ply specimen was 138,374 psi. The strength of specimens with low and intermediate level impact damages were 122,292 psi and 73,775 psi respectively, which amounted to 12% and 46% strength reduction. Plots of the number of acoustic emission events versus stress for both specimens with and without impact damage are shown in Figure 22. The total number of events or the rate of increase of those events are not reliable indicators of specimens' strength or approaching failure. The total number of events varied widely among the specimens. Similar variation of cumulative acoustic emission events at

the time of failure was found for impact damaged specimens as well. Hence, a better indicator of the final failure of the structures is needed to serve as a structural health monitoring tool.

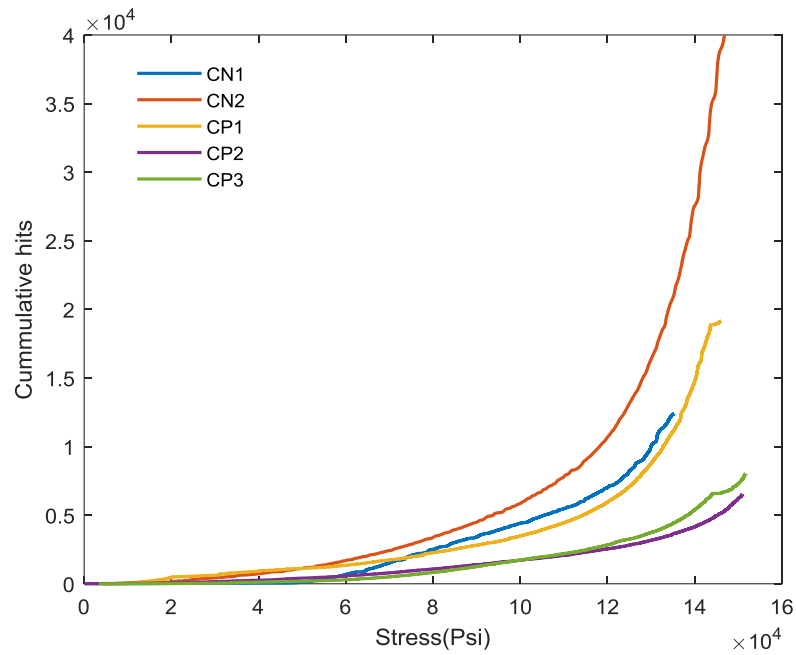


Figure 22. Cumulative number of acoustic emission events versus stress for specimen without initial impact damage.

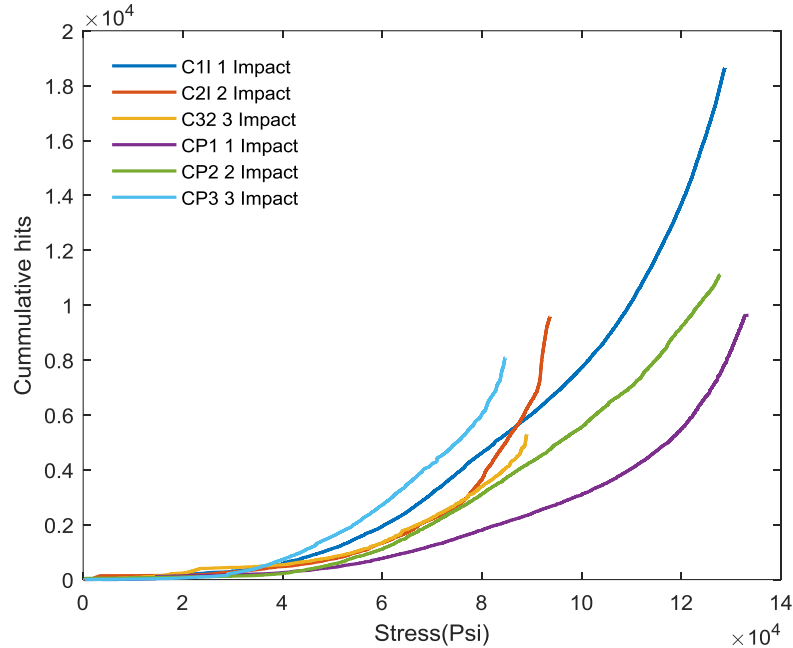


Figure 23. Cumulative number of AE events versus stress for specimen with initial impact damage.

4.4.1 Frequency content of acoustic emission events. While a few events had narrow frequency content, a large fraction of the waveforms had a wide range of frequencies. When examining these categories and the cumulative number of events in each category, the fact that higher end of the frequency components attenuates extremely rapidly while the lower frequency components travel long distances. While the 50 mm spacing between the sensors may be adequate for example for 300 kHz S_0 mode occurring anywhere in between the two sensors, we may lose most signals with 1 MHz frequency content that occur between the two sensors. When signals with wide spectral content is encountered, they need to be interpreted based on the attenuation they might have undergone before reaching the sensor. The information on the estimated amplitude and frequency ranges of acoustic emission signals for each of the failure modes gathered from the literature reviewed as well as the experimental results collected are summarized in Table 1. Since direct measurement of amplitude and frequency content of

acoustic emission signals from specific failure mode is unavailable, estimates of expected parameters are used to interpret the experimental data. The amplitudes and frequency ranges within the same failure mode will change based on the source to sensor distance, the crack velocity, stress level, and the location of the failure relative to the neutral axis of the specimen. Hence, the estimate provided in Table 1 must be taken as a first approximation.

Table 1.

Estimated ranges of amplitudes and frequencies for the three failure modes

Failure mode	Stress magnitude	Participating area	Strain energy release	Duration of failure event	Estimate of frequency content	Estimate of amplitude	Lamb wave mode
Matrix cracks	Moderate	Order of 0.1 mm ²	Large	Moderate duration	200 to 500 kHz	Large	S ₀
Delaminations	Low	Order of 0.1 mm ² to 1 mm ²	Moderate	Longer duration	100 to 200 kHz	Very large	A ₀
Fiber breaks	High	Order of 0.001 mm ²	Small	Less than 1 microsecond	Up to 1 MHz	Small	S ₀

Hence to categorize such events their waveforms were filtered using three different bandpass filters, namely, 100 – 200 kHz, 300 – 600 kHz, and 600 – 2000 kHz, and their respective peak amplitudes were determined. The ratios of these filtered waveform to original amplitude were determined to classify them into three groups. These were termed low frequency, mid-frequency, and high frequency events. Since, the high frequency components had extremely high attenuation rate, events which had amplitudes greater than 10 mv were classified as high frequency events even though their low frequency or mid frequency amplitudes were higher. Of

the remaining waveforms the events were grouped as either low frequency events or mid frequency events based on the amplitudes of their filtered signal amplitudes. Figures 24 and 25 show the plots of number of events versus applied stress that indicates the rate of increase of events belonging to each category for the cross-ply specimen without initial damage. In other undamaged specimens, the cumulative number of low and mid frequency events exceeded that of high frequency events. Similar plots for specimens for low level of impact damage and high level of impact damage are shown in Figures 26 and 27.

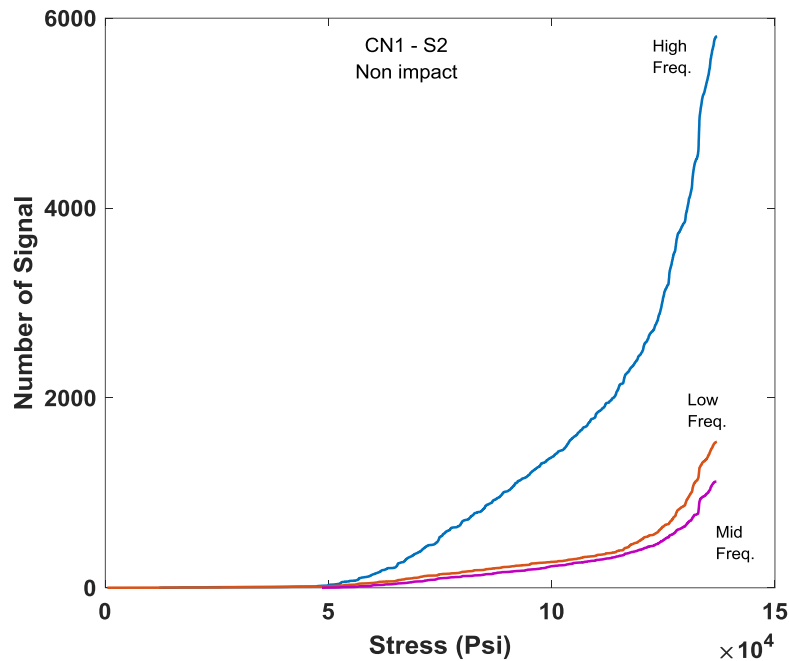


Figure 24. Acoustic emission events classified based on dominant frequency content for specimen CN1 without initial damage.

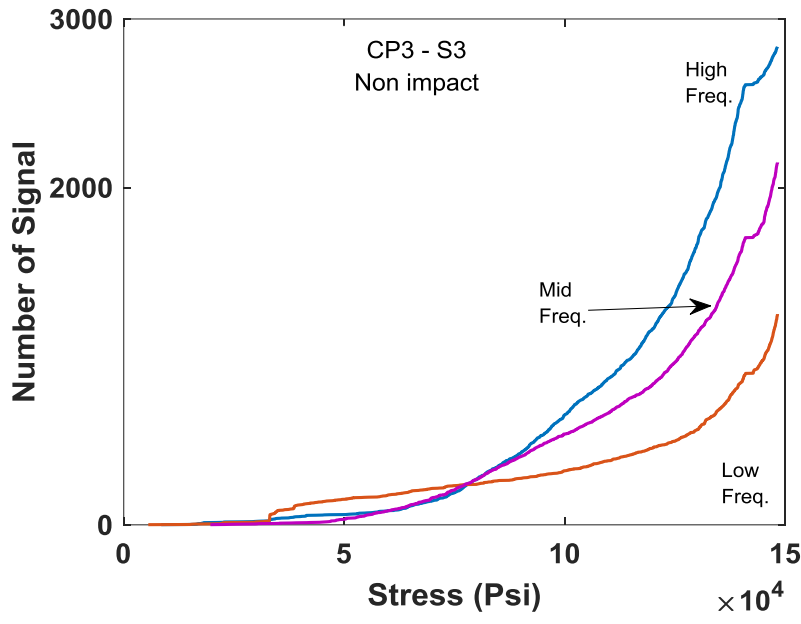


Figure 25. Acoustic emission events classified based on dominant frequency content for specimen CP3 without initial damage.

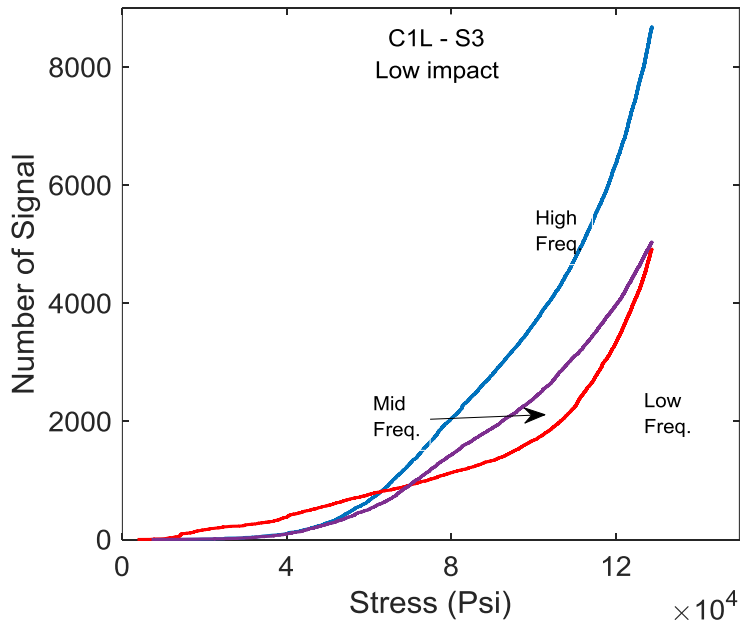


Figure 26. Acoustic emission events classified based on dominant frequency content for specimen with low level of initial impact damage.

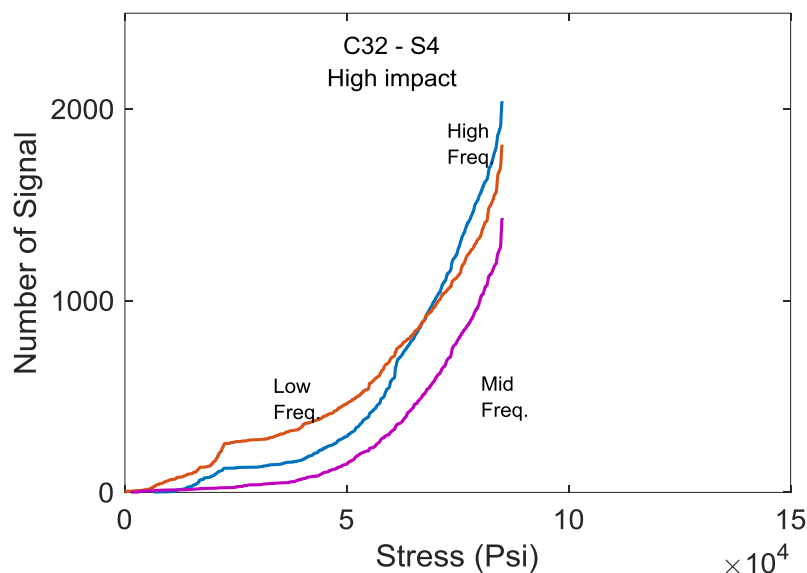


Figure 27. Acoustic emission events classified based on dominant frequency content for specimen with high level of initial impact damage.

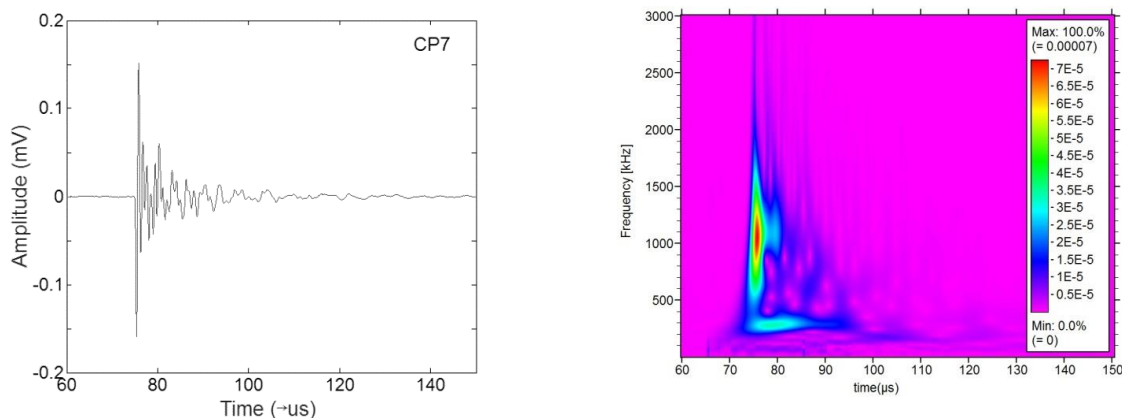


Figure 28. Waveform and corresponding wavelet diagrams for a representative high frequency AE signals from cross-ply specimens.

In both undamaged as well as impact damaged specimens, acoustic emission signals with frequencies well in excess of 1 MHz were seen, mostly in the last 30% of the loading cycle. Such waveforms are presumed to originate from fiber break events. Representative waveforms belonging to this category is shown in Figure 28. In a few of the specimens, a small number of

high frequency events started appearing at about 25% of the ultimate stress, and the number of these high frequency events gradually increased. This rate rapidly increased beyond 70% of the ultimate stress.

Two sets of 6 successive acoustic emission signals and their FFT are shown in figures 29 and 30 to illustrate the fact at a given point in the load history successive events with widely different frequency content occur and the bonded piezoelectric sensors are able to faithfully record them irrespective of their frequency content. The first set of waveforms were obtained from a specimen without initial damage and at 30% of ultimate stress. Some of these events have frequencies extending to 1500 kHz while others have frequencies of less than 300 kHz. Similar situation is seen in figure 31 and 32 for 6 successive events recorded at 90% of the ultimate stress. On the average these events had higher frequency content.

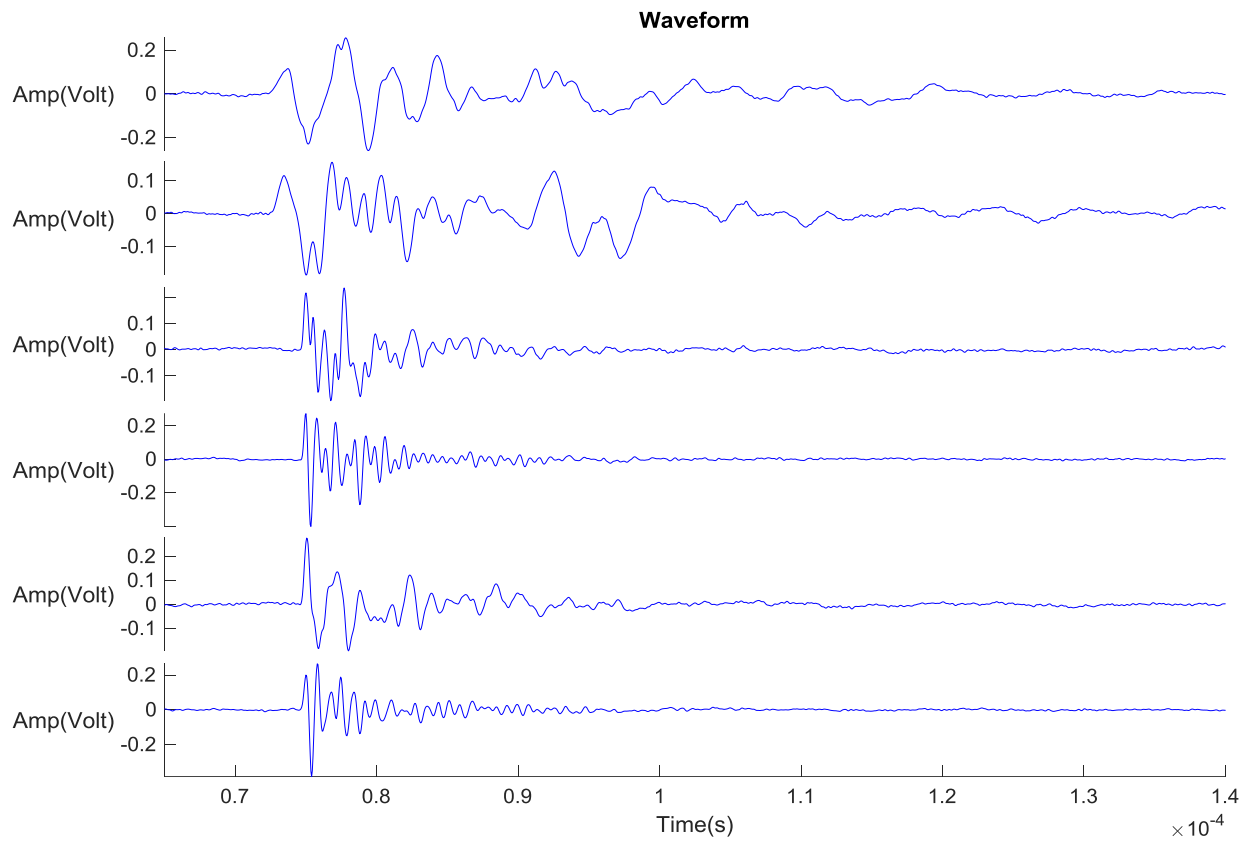


Figure 29. Waveforms corresponding to successive acoustic emission events at 30% of ultimate stress for CN1.

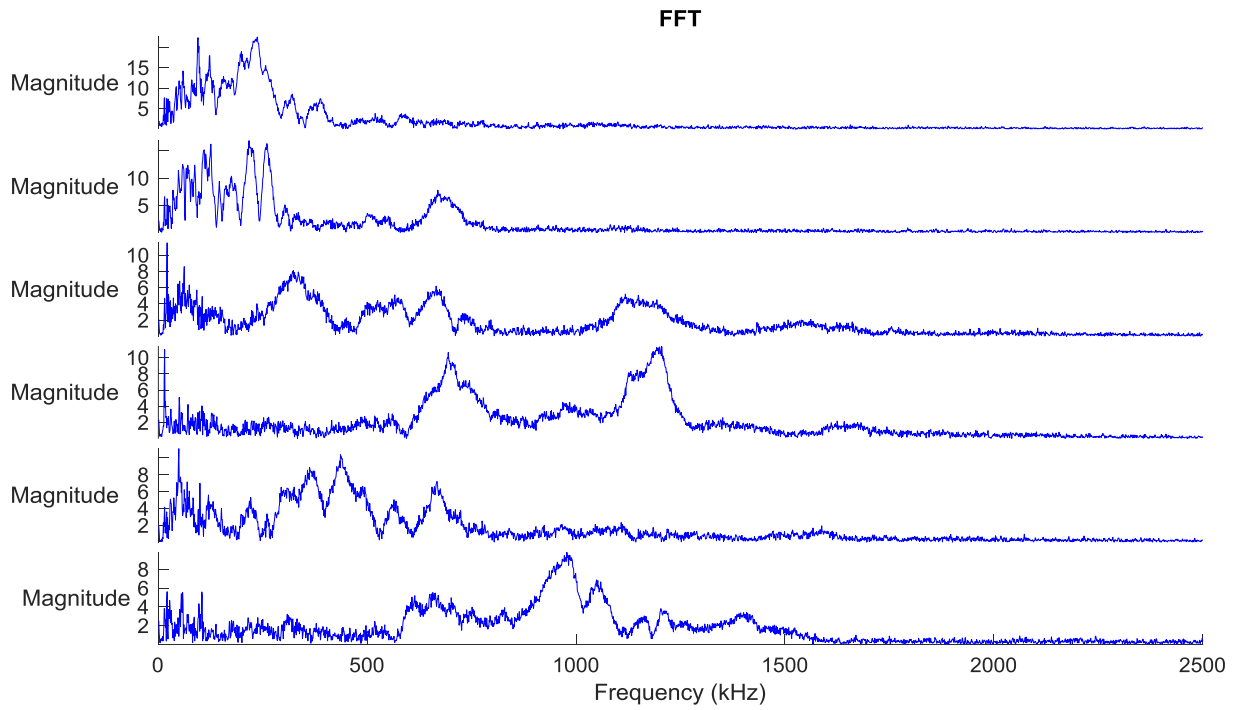


Figure 30. Frequency content of successive acoustic emission events at 30% of ultimate stress for CN1.

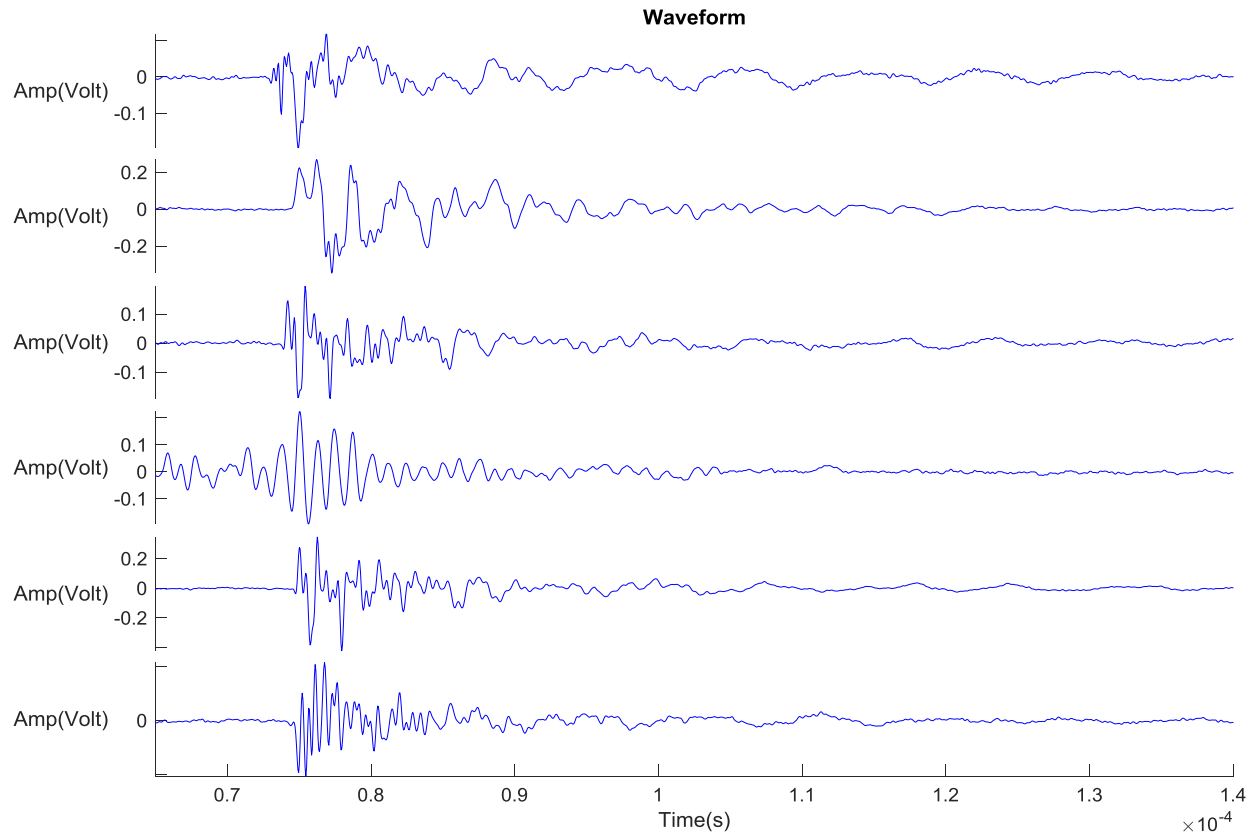


Figure 31. Waveforms corresponding to successive acoustic emission events at 90% of ultimate stress for CN1.

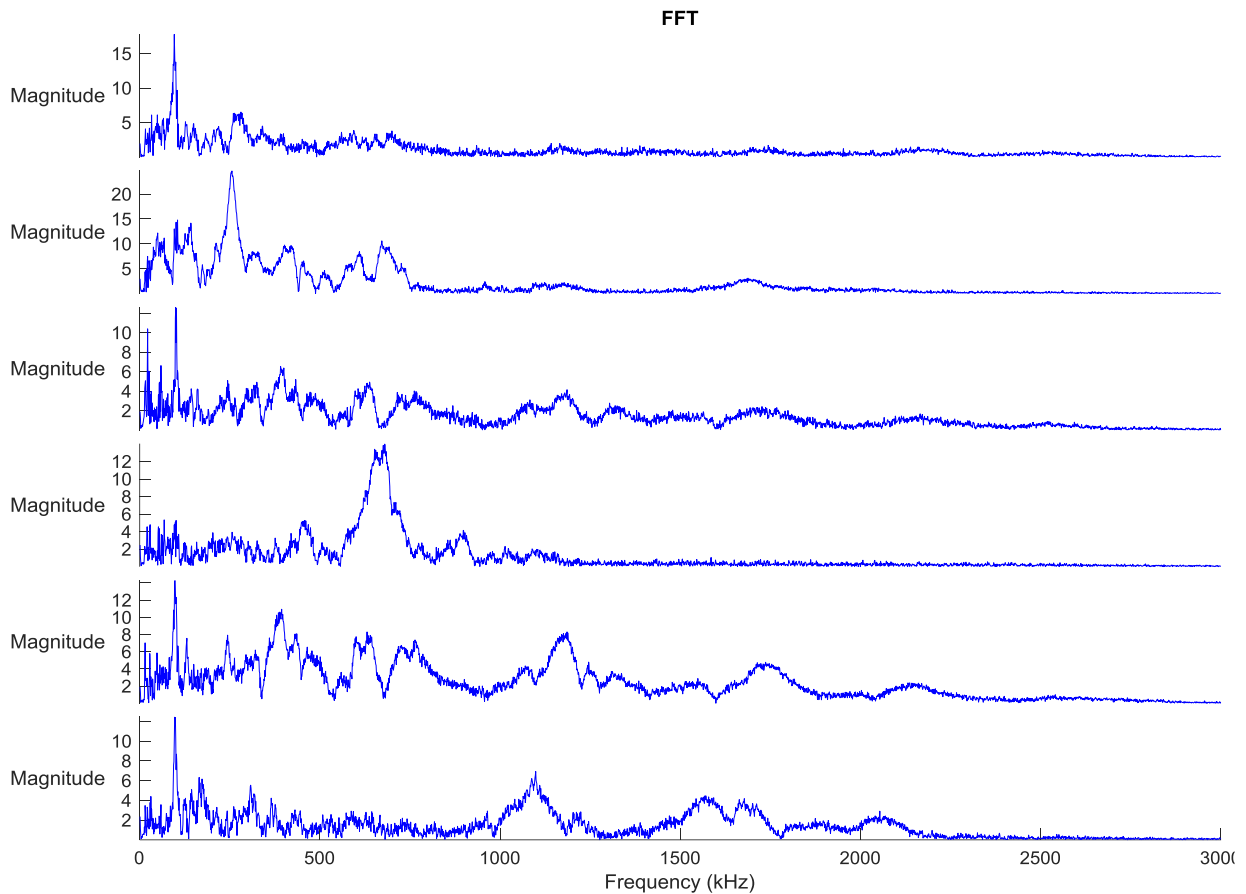


Figure 32. Frequency content of successive acoustic emission events at 90% of ultimate stress for CN1.

4.5 Classification of Acoustic Emission Events Based on the Waveform and Frequency Content

While a few events had narrow frequency content, a large fraction of the waveforms had a wide range of frequencies. Hence to categorize such events their waveforms were filtered using three different bandpass filters, namely, 100 – 200 kHz, 300 – 600 kHz, and 600 – 2000 kHz, and their respective peak amplitudes were determined. The ratios of these filtered waveform to original amplitude were determined to classify them into three groups. These were termed low frequency, mid-frequency, and high frequency events. Since, the high frequency components had

a very high attenuation rate, events which had amplitudes greater than 10 mv were classified as high frequency events even though their low frequency or mid frequency amplitudes were higher. Of the remaining waveforms the events were grouped as either low frequency events or mid frequency events based on the amplitudes of their filtered signal amplitudes.

4.5.1 Low and intermediate frequency events. Associating acoustic emission waveforms with the failure event has been attempted by numerous researchers in the past but there has been little consensus and no direct one to one evidence to support the classification. Based on the direction of excitation with respect to the specimen axis and the estimated duration of the crack propagation within such a failure event one may speculate the probable source of such an event. Cross ply laminate configurations and the type of damage as a function of quasi-static load level reported in the literature are examined in this section. The experimentally observed behavior of $[0/90_m]_n$ has been documented by several researchers [Jamison 1986, Talreja 1985, Boniface et, al, 97, Yokozeki 2005, Sing and Talreja 2010, Berthelot 2003, and Ogiwara et.al., 1995]. Here 'm' is the lumped 90-degree plies and 'n' is the number of repeating lamina configurations within the symmetric laminate. These laminates' final failure is determined by the failure of 0-degree plies that are aligned with the uniaxial load. However, such laminates undergo extensive damage to the 90 laminae in the form of transverse cracks and can also have delaminations at the interface between 0 and 90 layers, initiating from the tips of the transverse matrix cracks in 90-degree layers. The rate at which these transverse matrix cracks appear until the final failure is strongly dependent on the number of 90-degree laminae grouped together. For laminate with $m = 1$, similar to the specimen that is examined in this study, transverse matrix cracks appear relatively late at 30% of the ultimate stress and increase in number at an exponential rate until the final fracture. This rate at which these transverse cracks

form is dependent on the rate of loading, and often hold periods in excess of 30 second are required to complete the formation of the transverse cracks at a given load level because the matrix is viscoelastic [Jamison 1986]. Further for laminae with $m=1$, the transverse crack initiate late compared with laminates where m is large and propagates across both the ply thickness and along the specimen width gradually [Boniface 1997]. Acoustic emission events durations are measured in seconds while the formation of transverse cracks may take several tens of seconds or more. Hence, a single matrix crack can give rise to several acoustic emission signals. Transverse matrix cracks generally originate near the free edge and grow inward, and based on theoretical models, can give rise to significant energy release. Some researchers have found that no or modest delaminations growth in laminates with single 90-degree plies interspersed between 0-degree laminae [Jamison 1986, Takeda 1995]. Others have found significant delamination growth in this laminate configuration [Garcia et. al., 2019]. Based on the experimental data available from the literature, we can speculate that a some of the acoustic emission events in lower end of the frequency range (100-200 kHz) may originate from delamination events particularly if they are of long duration. We have to consider the fact that edge replica and dye penetrant methods used to locate and measure the delaminations have limitations in terms of accounting for such damage throughout the volume of the specimen, while the low frequency acoustic emissions from delaminations anywhere in the specimen can be picked up by AE sensors. Most of the intermediate frequency (300-600 kHz) and some of the low frequency (100-200 kHz) range events are likely to be originated by either the initiation or propagation of transverse crack events.

4.5.2 High frequency events. Duration of fiber fracture events are expected to be very short because of the diameter of the carbon fiber is less than 0.010 mm, the crack velocity in

such fibers are expected to be large because of the high elastic modulus of the fiber and high stresses at which these breaks occur. In contrast the width and length of a transverse matrix crack is likely to be tens or hundreds of times larger than the fiber diameter, and the crack velocity in the transverse matrix cracks are likely to be considerably smaller because of the smaller elastic modulus and smaller stress that is driving the crack growth. Hence it is reasonable to expect that the highest frequency events that are seen in these tests are from fiber fractures. Such acoustic emission events were observed during the tests of specimens having only 0-degree laminae, and the only failure mode in such specimens were fiber breaks [Mills-Dadson, 2015].

Most acoustic emission results reported in the literature have used conventional acoustic emission sensors whose response was limited to about 700 kHz because of their frequency response or the aperture effect. They are also sensitive to out of plane displacements to detect acoustic emission signals. The bonded acoustic emission sensors used in this study on the other hand have frequency response in excess of 2 MHz and are sensitive to the in-plane strain induced by the acoustic emission waves, and hence are inherently more sensitive to symmetric modes. These characteristics make the bonded piezoelectric sensors used in this study better positioned to capture high frequency symmetric waves resulting from fiber breaks. As per the fiber strength statistics, and other experimental observations fiber failures are expected only after 70% load in significant numbers. In figure 25, fiber fractures are seen to start at load level of about 30% of the ultimate strength. Possible reasons may include the significant increase in attenuation particularly to high frequency signals as the damage in the specimen in the form of matrix cracks and delaminations accumulate at higher load levels.

4.6 Detecting the Formation of Clusters of Adjacent Fiber Breaks

As described earlier [Jamison 1986, Scott et. al., 2011, Rosini et. al., 2018] the formation of adjacent fiber breaks, in which the cluster of fibers are known to form close to the final fracture of composite specimens. The formation of such clusters are precursors to the onset of unstable damage growth that lead to the final fracture. This transition from stable damage growth in the form of isolated fiber breaks to the formation of near simultaneous clusters of adjacent fiber breaks is analogous to stable incremental crack growth to rapid crack growth in isotropic materials as the crack approaches critical size for the prevailing stress level. This transition is expected in undamaged structures when the ultimate strength of the material is reached but can also occur at lower load levels if the structure experienced unexpected events such as impact damage. Hence, it becomes essential to have structural health monitoring technique that can provide timely warning of the formation of such cluster of fiber break and the impending failure.

Identifying the formation of such clusters of fiber breaks based on acoustic emission event locations with adequate resolution is not feasible with the current capability of acoustic emission technique. Alternative means of identifying acoustic emission signals that originate from nearly the same location in terms of the scale of fiber diameters is needed. Close examination of acoustic emission waveforms that were recorded close to the final fracture of specimens revealed that several groups of successive AE waveforms were almost identical in shape. These groups of identical waveforms appeared mostly close to the ultimate load. Members of these groups appear in rapid succession, and almost at the same load level. Often, two such waveforms appear in 100 or 200 microseconds apart. In addition, the number of such individual groups of near identical waveforms rapidly increases as the specimen failure is approached [Whitlow, 2013, Mills-Dadson 2016]. These groups of identical waveforms appear

to be emanating from the formation of adjacent fiber breaks, or the so called ‘multiplets.’ If acoustic emission signals are caused by the same type of sources (fiber breaks), and if the source location is same or nearly same (adjacent fibers in a cluster), and if the propagation path and medium remain the same (the state of damage at this load level), the shape of AE waveforms should remain the same. Since, the diameter of a group of fibers that belong to multiplets of that includes 20 or less members is very small (less than 0.1 mm) compared to the wave length of the stress waves detected and the specimen size as well as the AE propagation distance, these conditions are satisfied.

After examining a very large number of waveforms obtained from these composite specimens, waveforms that were nearly identical and occurring in rapid succession, were grouped. Correlation among large groups of waveforms was used to automatically locate and isolate such clusters of near identical waveforms. Figure 33 shows the plots of the number of clusters as a function of applied stress level for several specimens. Each circle in these figures indicates a group of near identical acoustic emission waveform that was detected at that load level. The number of identical acoustic emission signals within that group at that load level is proportionally indicated by the size of each circle as well as its color. As the load increases, additional groups were seen to form, and the rate of their formation increased with load level. Further, the size of the cluster of identical waveforms also increased as the ultimate load was approached, as indicated by the changes in the diameters in these figures. It is hypothesized that the formation and growth of these groups of AE waveforms correspond to the clusters of fiber breaks which mark the transition from stable damage growth to unstable damage growth. The appearance of such clusters of identical waveforms are plotted for another undamaged specimen, namely CP3, in Figure 34. For this specimen, the number of such clusters are fewer, but near

final failure, the rate of appearance of such clusters become steeper indicating that the final failure is close.

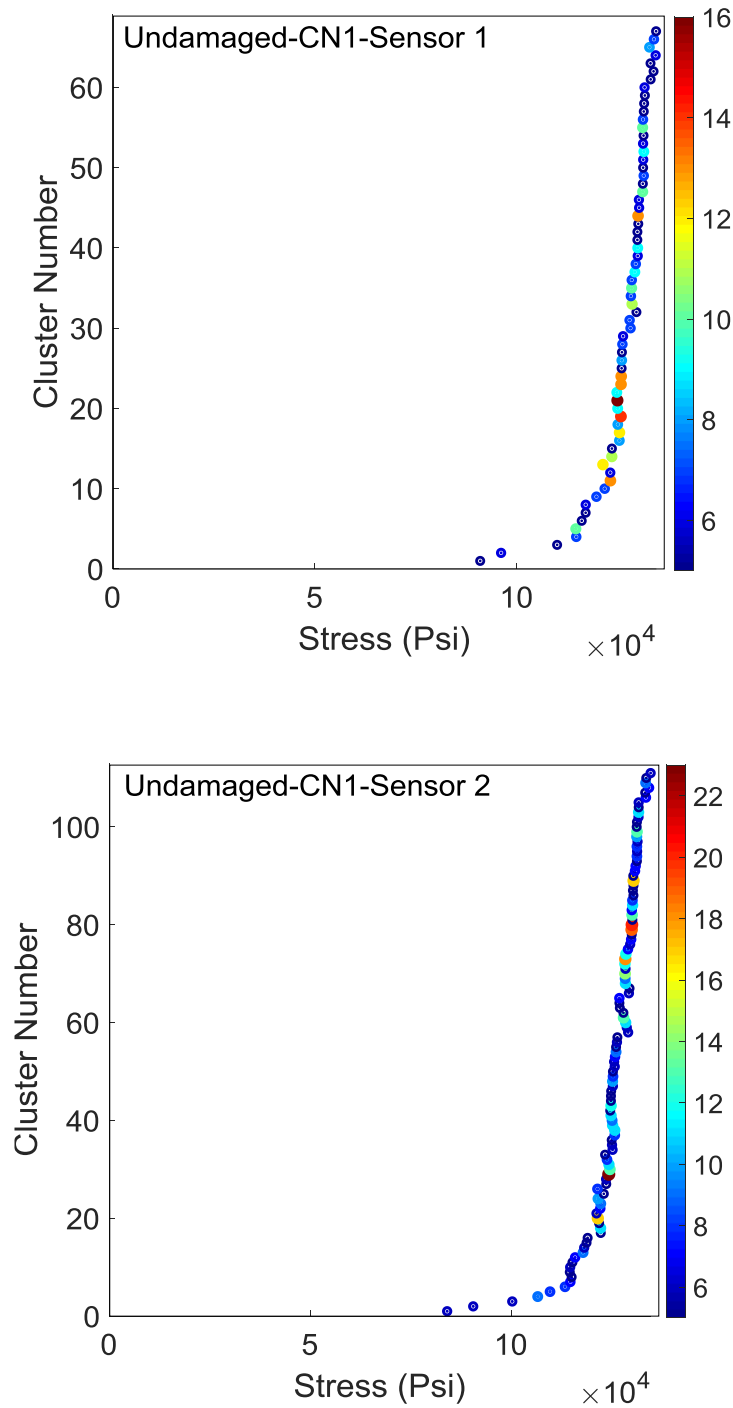


Figure 33. Clusters of identical waveforms in undamaged specimen CN1.

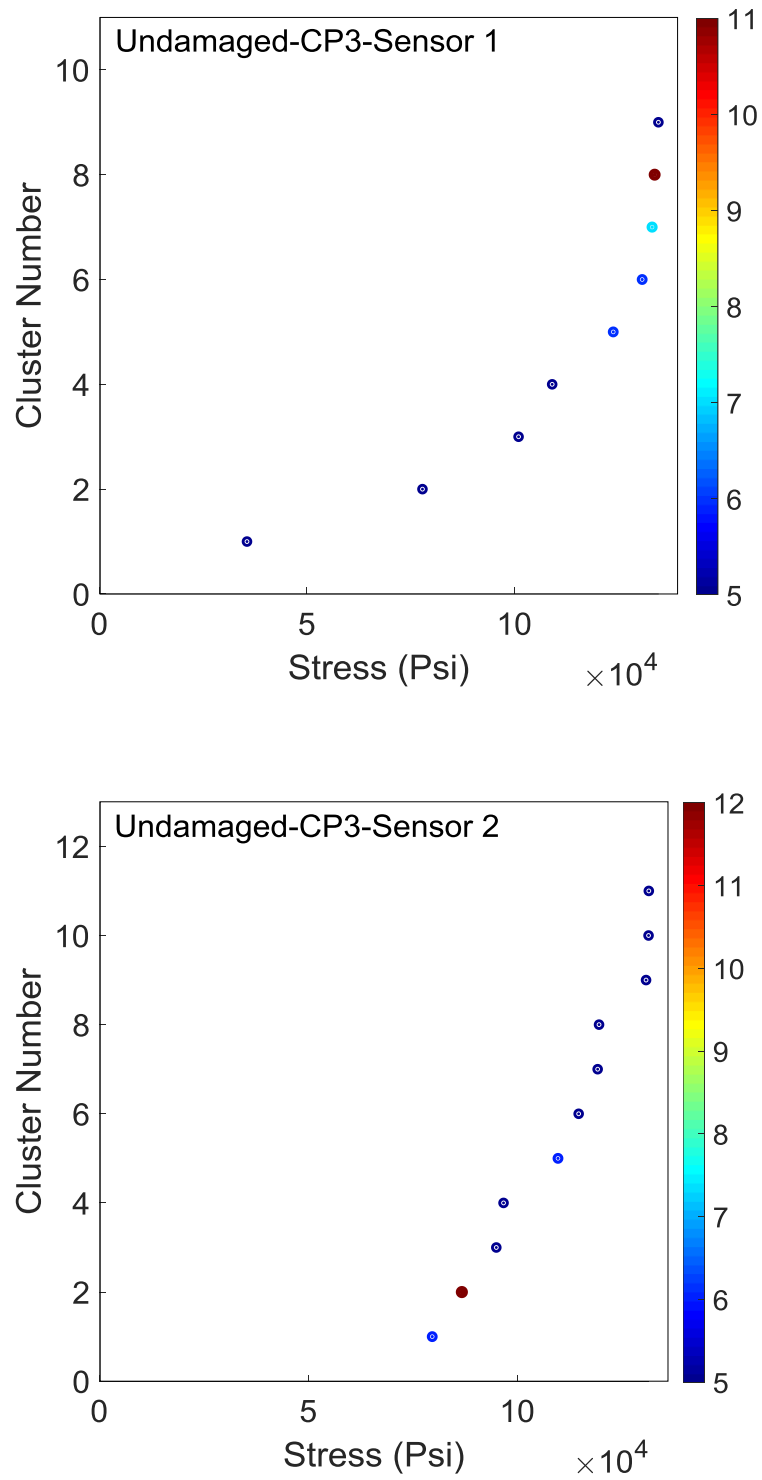


Figure 34. Clusters of identical waveforms in undamaged specimen CP3.

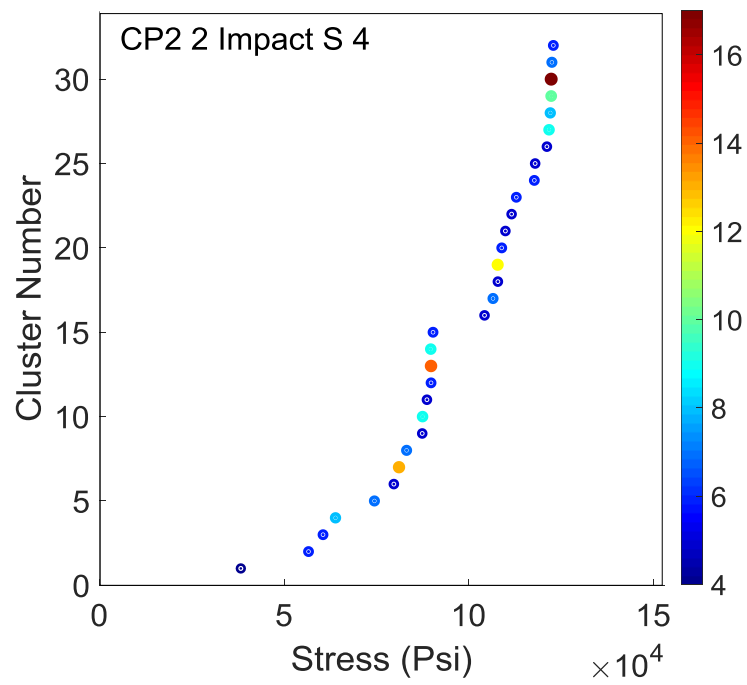
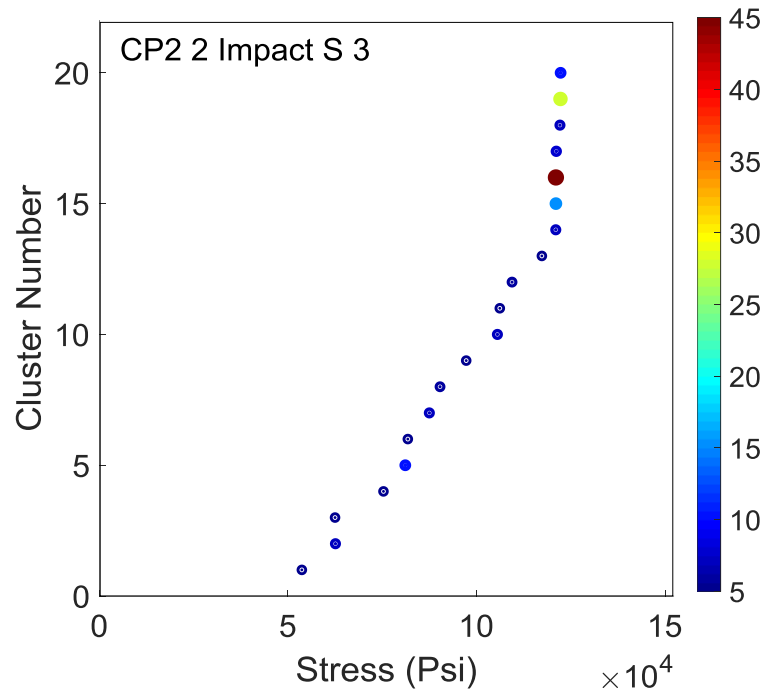


Figure 35. Clusters of identical waveforms in specimen with low level impact damage-CP2.

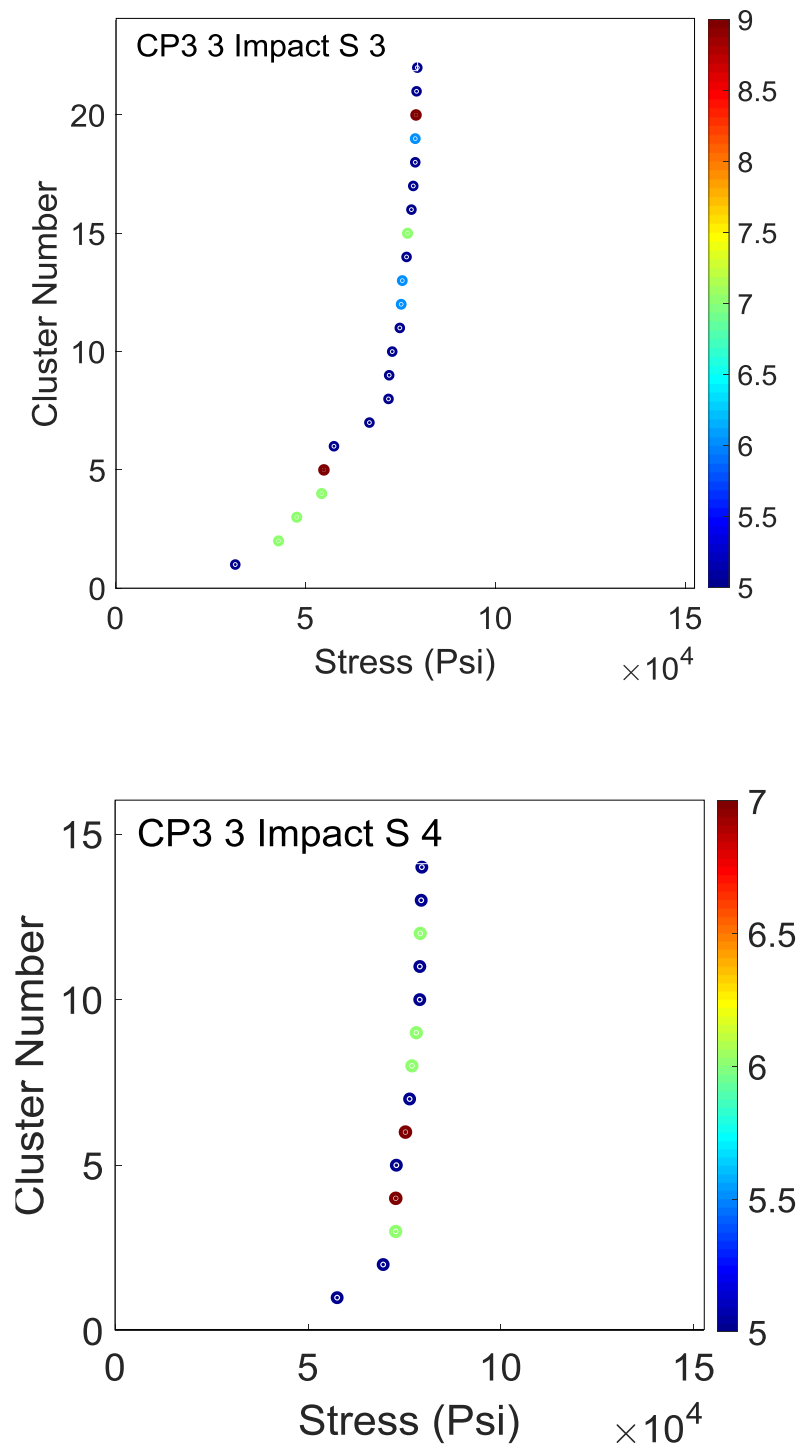


Figure 36. Clusters of identical waveforms in specimen with high level impact damage-CP3.

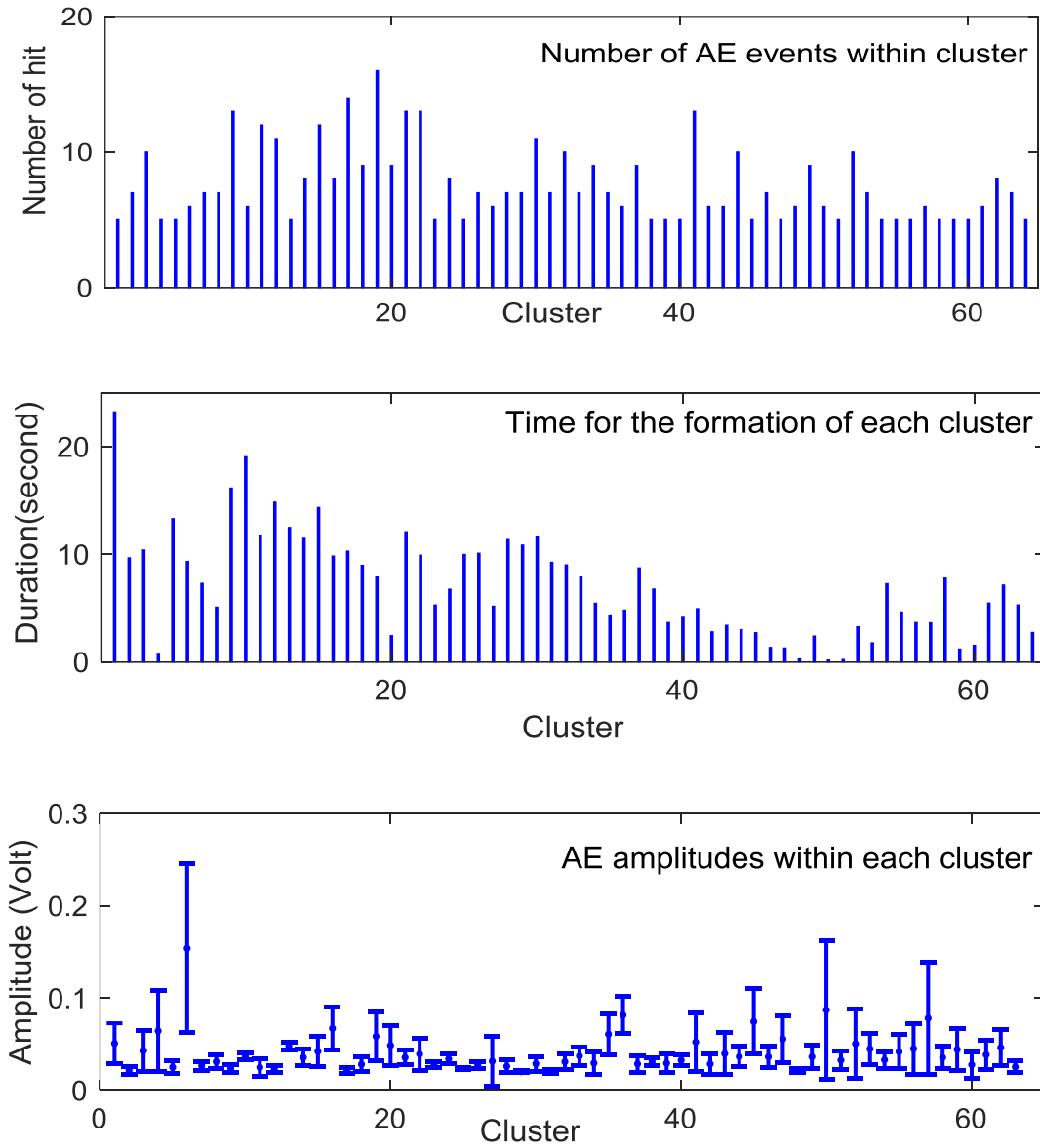


Figure 37. Cluster size, time to form and range of acoustic emission amplitudes within each cluster for CN1 specimen.

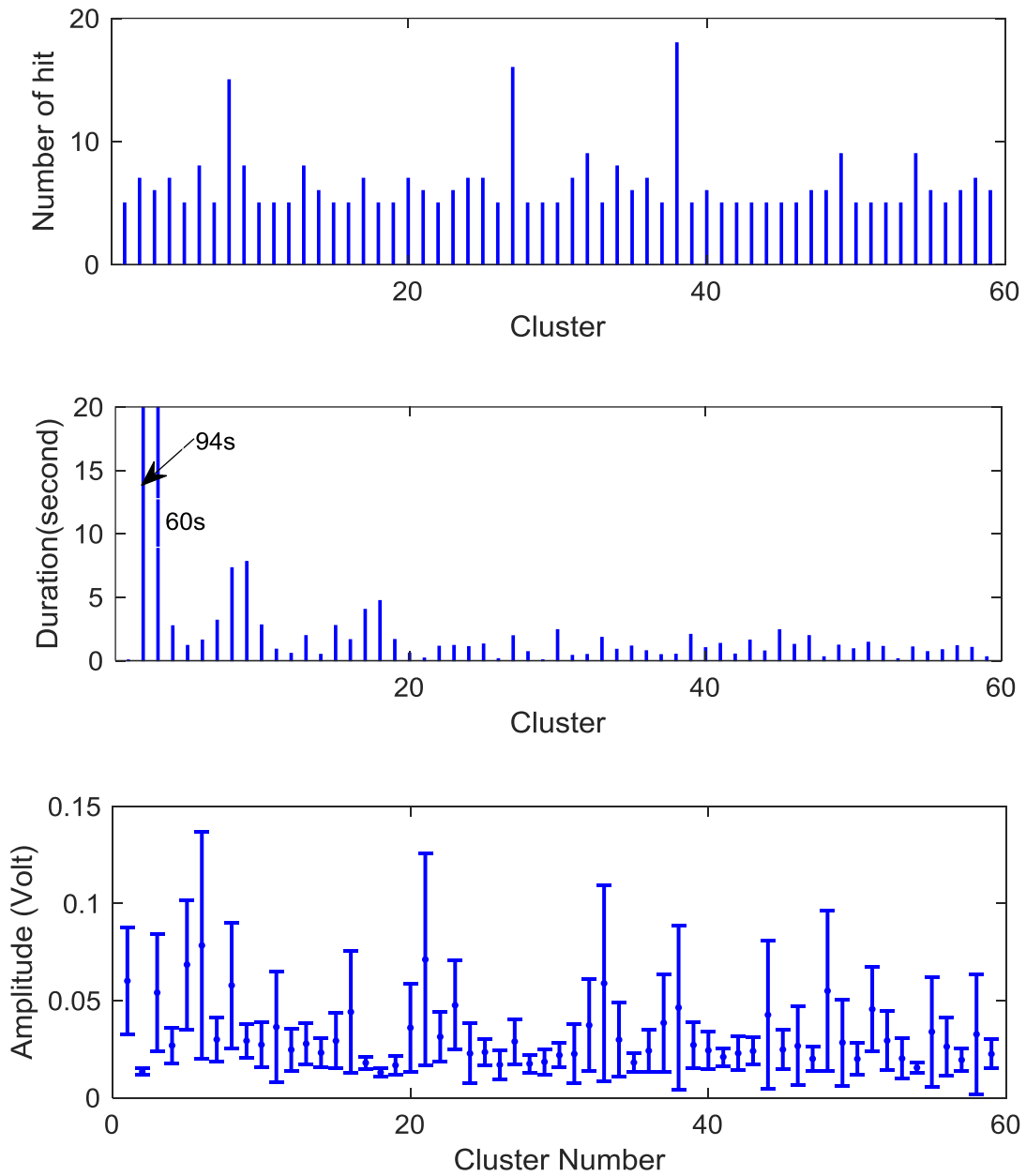


Figure 38. Cluster size, time to form and range of acoustic emission amplitudes within each cluster for CN2 specimen.

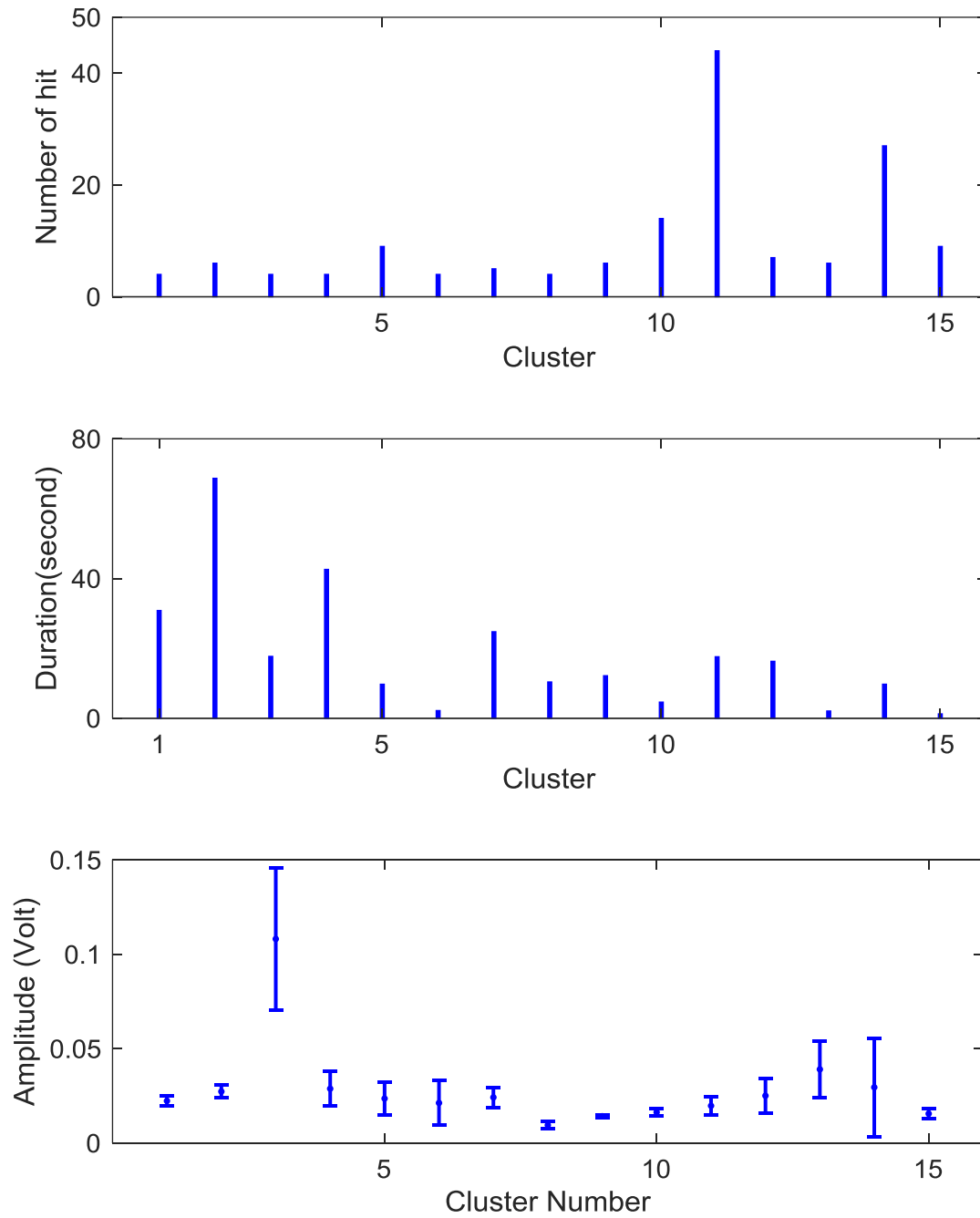


Figure 39. Cluster size, time to form and range of acoustic emission amplitudes within each cluster for with initial 2 impacts damage CP2 sensor 3.

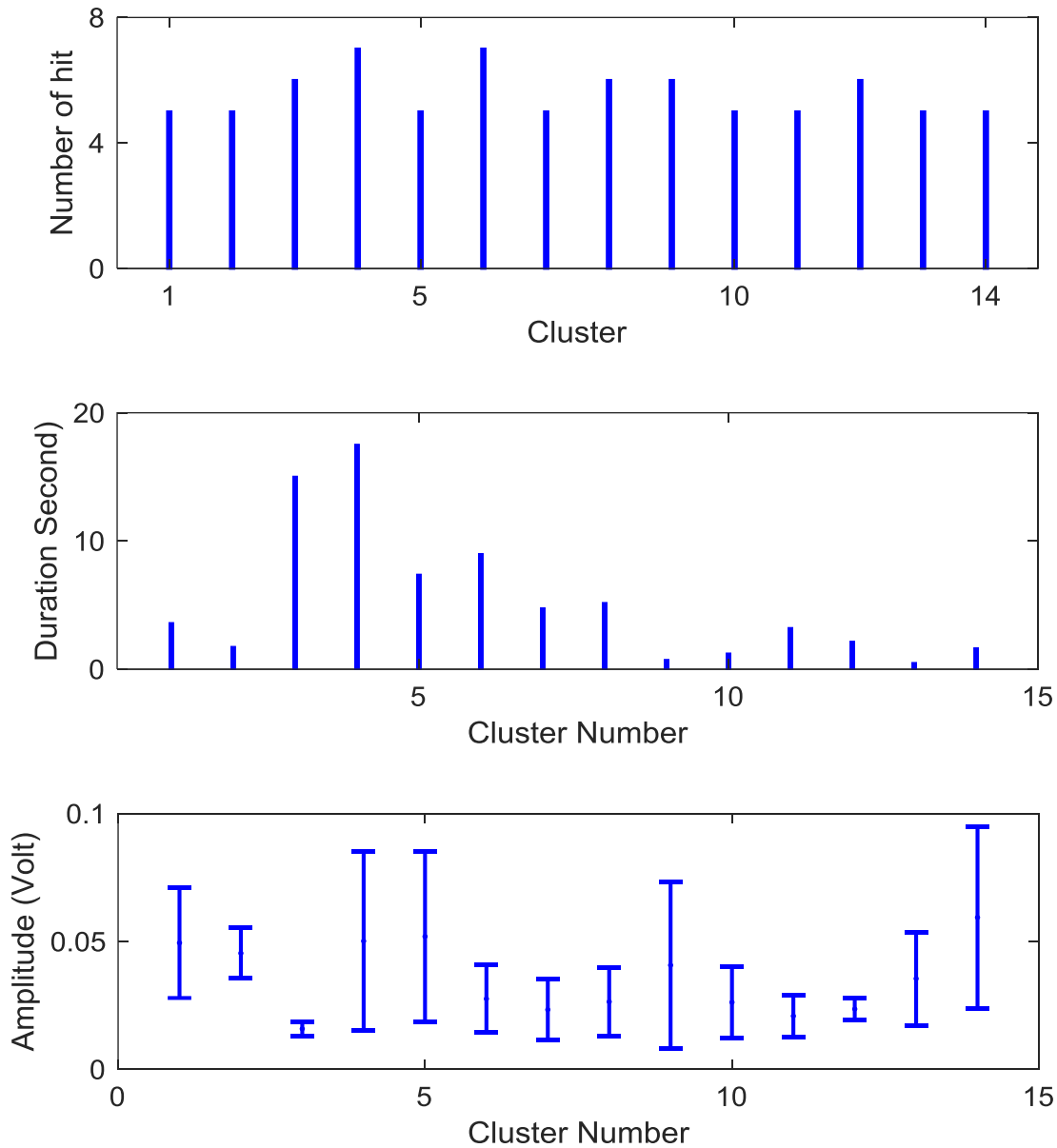


Figure 40. Cluster size, time to form and range of acoustic emission amplitudes within each cluster for with initial 3 impacts damage CP3 sensor 4.

Figures 35 and 36 correspond to specimens with initial impact damage. Specimen CP2 was subjected to a single impact before the static loading, while specimen CP3 was subjected to three impacts. As expected, the strength reduction for specimen CP2 was modest while for CP3

it was substantially higher. The formation of clusters of near identical waveforms increased as the applied load was approaching the final failure in both cases.

To understand the nature of transition from stable damage growth within the primary load carrying 0-degree laminae in the form of random fiber breaks to the unstable damage growth that results in the formation of clusters of adjacent fiber breaks the details of the members within each cluster of identical acoustic emission waveforms (i.e., the waveforms that make up each circle in the plots such as Figure 33 are examined. For example, in Figure 33, there were in excess of 66 groups of identical acoustic emission waveforms. The range of amplitudes within each group, the time difference between the first and the last acoustic emission event within a group, and number of acoustic emission events in each group were determined and plotted in Figures 37 to 39. The range of amplitude of these acoustic emission events were between 0 and 0.1 volts, but this range appeared to increase as the final failure is approached. The time between the first acoustic emission event and the last event within each group ranged from about 1 second to 30 seconds in Figure 38. It is significant that this time interval between the first event to the last event (which appears to be related to growth of cluster of adjacent fiber breaks from one to the max number) rapidly decreases as the final failure is approaching. The number of acoustic emission events within each group of waveforms is ranging from about 15 to 5. These results may be related to the direct CT observation of fiber failures of miniature cross-ply specimens from Scott et. al., 2011, and Rosini et. al., 2019. In their study Scott et. al. found the largest clusters of fiber breaks was made up of 14 adjacent fiber breaks. Since the specimens tested for the current study is at least an order of magnitude larger, we may expect clusters of even larger size. Rosini et. al. was able to record the damage state in their specimen at much closer intervals of load increment. Based on these observations Rosini deduced that when multiple fiber breaks

appear, they appear instantaneously, and not sequentially. If the hypothesis that identical acoustic emission waveforms emanate from clusters of adjacent fiber breaks, the present study contradicts that clusters of fiber breaks are formed sequentially, but they are significantly different from random isolated fiber breaks. The first fiber break within the cluster is closely followed by other neighbors and the cluster of broken fibers are completed within 5 to 10 seconds interval.

CHAPTER 5

Summary and Discussions

5.1 Acoustic Emission Wave Propagation in Isotropic Plates

Acoustic emission waves generated by a central crack in a thin aluminum plate was analyzed using finite element analysis. The propagation characteristics including the change in the amplitude of these waves with radial and angular change in the position of the sensing location was analyzed in detail. An important aspect of this study is the detailed characterization of the shear horizontal mode of the Lamb wave that is generated by simulated crack growth. The results presented indicate that the amplitude of the shear horizontal mode remains larger than the symmetric mode generated by a simulated through the thickness crack at the center of the plate. Design of a suitable sensor that can take advantage of this mode is challenging. New types of sensors were examined for this purpose. These sensors were reasonably successful in the experiments that employed simulated acoustic emission sources. However, they were not able provide good signals for detecting crack growth related SH modes during a fatigue crack growth experiment.

5.2 Different Damage Modes in Composite Materials and the Onset of Critical Damage

While polymer matrix composite materials are superior to conventional metallic materials for aerospace applications, they have one important vulnerability in terms of significant strength reduction due to impact damage. There is a need for a structural health monitoring technique that can provide advance warning of impending failure caused by such damage. In most composite laminate configurations, the structural failure is triggered by the formation of clusters of fiber breaks both in undamaged structures as well as those which have initial impact damage. The onset of such damage progression in CFRP structural members in tension is the focus of this

paper. The formation of such clusters of fiber breaks in most cases was found to start at 70% of ultimate strength or later.

Acoustic emission technique has the potential to quantify damage in composite materials, but it has not been found to reliably foretell impending failure or indicate the failure mode corresponding to individual events. One of the major factors holding back the potential of the acoustic emission technique is the limitation of acoustic emission sensors currently in use that are related to their inability to capture important high frequency components. New sensors with frequency response in excess of 2 MHz were further developed and used in this research. Further, since important information about the failure modes are lost because of the high attenuation seen in composite structures, the source to sensor distance was maintained small by using a denser array of sensors.

The structural integrity and strength of cross-ply laminates are fiber dominated properties [Reifsnider and Case, 2001] that are controlled by the 0-degree laminae that are aligned in the major load direction. Onset of critical damage leading to final structural failure in these laminates occur in the form of clusters of fiber breaks. Hence in structures that have this configuration, it is essential to monitor the formation of clusters of fiber breaks. Acoustic emission response of cross-ply carbon-epoxy composite specimens with initial impact damage was studied to determine if acoustic emission technique can detect the presence of this damage and serve as an effective structural health monitoring technique to provide timely warning of the onset of critical damage in such specimens. Currently available commercial acoustic emission sensors are limited to about 700 kHz because of their frequency response and the aperture effect. In our studies we found acoustic emission signals extending to 2 MHz, nearly three times the frequency range reported in most available acoustic emission studies. Extensive literature search

was made to understand the failure process in cross-ply laminates and the acoustic emission results from the current study was interpreted based on the information gathered from the literature. To relate the acoustic emission signals to the failure mode, acoustic emission waveforms were separated into three categories, namely, those which had dominant amplitudes in the ranges 100 – 200 kHz, 300 to 600 kHz, and 600 – 2000 kHz. As discussed in the previous sections, most of the intermediate frequency (300-600 kHz) and some of the low frequency (100-200 kHz) range events are likely to be originated by either the initiation or propagation of transverse crack events. Some of the low frequency signals are likely to be due to delaminations. The signals with high frequency components beyond 600 kHz and with relatively low amplitudes are likely to be originating from fiber fractures.

Since the appearance of clusters of fiber breaks separates marks the transition of stable damage growth to unstable damage propagation, it is necessary to differentiate random fiber breaks from clusters of adjacent fiber breaks. This objective was achieved by identifying events with near identical waveform occurring in rapid succession. Each group of such waveforms contain four to fifteen members. In both undamaged specimens and specimens with initial impact damage a steep increase in the number of clusters indicated the transition to critical damage. In these specimens the appearance of such clusters of waveforms parallel the formation of clusters of fiber breaks observed in composite specimens through SEM as well as computed tomography observations. This technique needs to be validated through more extensive tests so that it can be scaled up to monitor real life structures such as primary structures of aerospace vehicles.

References

1. Abrate, Serge. "Impact on laminated composites: recent advances." *Applied Mechanics Reviews* 47.11 (1994): 517-544.
2. Aggelis, D. G., et al. "Acoustic structural health monitoring of composite materials: Damage identification and evaluation in cross ply laminates using acoustic emission and ultrasonics." *Composites Science and Technology* 72.10 (2012): 1127-1133.
3. Asamene, K., L. Hudson, and M. Sundaresan, "Influence of attenuation on acoustic emission signals in carbon fiber reinforced polymer panels," *Ultrasonics*, 2015. 59: p. 86-93.
4. Asamene, Kassahun, and Mannur Sundaresan. "Analysis of experimentally generated friction related acoustic emission signals." *Wear* 296.1-2 (2012): 607-618.
5. ASNT Handbook Volume 6: Acoustic Emission Testing, Technical Editors: R. Miller and E.V.K. Hill, American Society for Non-destructive Testing, 2005.
6. Auld, B. A., 1990, *Acoustic Fields and Waves in Solids*, Vol. 1 and 2, Second edition.; Kreiger Publishing Co., FL.
7. Baker, Christopher, et al. "Transverse cracking in carbon fiber reinforced polymer composites: Modal acoustic emission and peak frequency analysis." *Composites Science and Technology* 116 (2015): 26-32.
8. Berthelot, Jean-Marie. "Transverse cracking and delamination in cross-ply glass-fiber and carbon-fiber reinforced plastic laminates: static and fatigue loading." *Applied Mechanics Reviews* 56.1 (2003): 111-147.
9. Boniface, L., et al. "Transverse ply cracking in cross-ply CFRP laminates—initiation or propagation controlled?" *Journal of Composite Materials* 31.11 (1997): 1080-1112.

10. Bull, D. J., S. M. Spearing, and I. Sinclair. "Investigation of the response to low velocity impact and quasi-static indentation loading of particle-toughened carbon-fibre composite materials." *Composites Part A: Applied Science and Manufacturing* 74 (2015): 38-46.
11. Crivelli, Davide, et al. "Localisation and identification of fatigue matrix cracking and delamination in a carbon fibre panel by acoustic emission." *Composites Part B: Engineering* 74 (2015): 1-12.
12. De Rosa, I.M., C. Santulli, and F. Sarasini. 2009. "Acoustic emission for monitoring the mechanical behaviour of natural fibre composites: a literature review," *Composites Part A: Applied Science and Manufacturing*, 40(9): 1456-1469.
13. Djabali, Abderrahmane, et al. "Fatigue damage evolution in thick composite laminates: Combination of X-ray tomography, acoustic emission and digital image correlation." *Composites Science and Technology* (2019): 107815.
14. Dzenis, Y.A. and J. Qian. 2001. "Analysis of microdamage evolution histories in composites," *International Journal of Solids and Structures*,. 38(10–13): 1831-1854.
15. García, I. G., et al. "Experimental study of the size effect on transverse cracking in cross-ply laminates and comparison with the main theoretical models." *Mechanics of Materials* 128 (2019): 24-37.
16. Gliszczynski, Adrian, Tomasz Kubiak, and Kamil Wawer. "Barely visible impact damages of GFRP laminate profiles—An experimental study." *Composites Part B: Engineering* 158 (2019): 10-17.
17. Graff, K. F., 1991, *Wave Motion in Elastic Solids*, Dover Publications Inc., New York.
18. H. Lamb, *On Waves in an Elastic Plate*, *Proceedings of the Royal Society of London. Series A*, 93 (1917) 114-128.

19. Highsmith, Alton L., and Kenneth L. Reifsnider. "Stiffness-reduction mechanisms in composite laminates." *Damage in composite materials: basic mechanisms, accumulation, tolerance, and characterization*. ASTM International, 1982.
20. Jacques, M., et al. "Evaluation of bonded piezoelectric AE sensor for structural health monitoring," in *The 15th International Symposium on: Smart Structures and Materials & Nondestructive Evaluation and Health Monitoring*. 2008. International Society for Optics and Photonics.
21. Jamison, Russell D. "On the interrelationship between fiber fracture and ply cracking in graphite/epoxy laminates." *Composite Materials: Fatigue and Fracture*. ASTM International, 1986.
22. Jamison, Russell D., et al. "Characterization and analysis of damage mechanisms in tension-tension fatigue of graphite/epoxy laminates." *Effects of defects in composite materials*. ASTM International, 1984.
23. Janapati, V., Kopsaftopoulos, F., Li, F., Lee, S. J., & Chang, F. K. (2016). Damage detection sensitivity characterization of acousto-ultrasound-based structural health monitoring techniques. *Structural Health Monitoring*, 15(2), 143-161.
24. Jang, Byeong-Wook, and Chun-Gon Kim. "Real-time detection of low-velocity impact-induced delamination onset in composite laminates for efficient management of structural health." *Composites Part B: Engineering* 123 (2017): 124-135.
25. Kirikera, Goutham R., et al. "A structural neural system for real-time health monitoring of composite materials." *Structural Health Monitoring* 7.1 (2008): 65-83.

26. Li, Li, Stepan V. Lomov, and Xiong Yan. "Correlation of acoustic emission with optically observed damage in a glass/epoxy woven laminate under tensile loading." *Composite structures* 123 (2015): 45-53.
27. M.R. Gorman, *Plate wave acoustic emission*, Journal of Acoustical Society of America, 90 (1991) 358-364.
28. M.R. Gorman, W.H. Prosser, AE Source Orientation by Plate Wave Analysis, *Journal of Acoustic Emission*, 9 (1991) 283--288.
29. Maillet, Emmanuel, et al. "Feasibility and limitations of damage identification in composite materials using acoustic emission." *Composites Part A: Applied Science and Manufacturing* 75 (2015): 77-83.
30. Marec, A., J.-H. Thomas, and R. El Guerjouma, "Damage characterization of polymer-based composite materials: Multivariable analysis and wavelet transform for clustering acoustic emission data," *Mechanical Systems and Signal Processing*, 2008. 22(6): p. 1441-1464.
31. McCrory, J.P., et al. 2015. "Damage classification in carbon fibre composites using acoustic emission: A comparison of three techniques," *Composites Part B: Engineering*,. 68(0): 424-430.
32. Mehdikhani, Mahoor, et al. "Multi-scale digital image correlation for detection and quantification of matrix cracks in carbon fiber composite laminates in the absence and presence of voids controlled by the cure cycle." *Composites Part B: Engineering* 154 (2018): 138-147.

33. Miao, Hongchen, Qiang Huan, and Faxin Li. "Excitation and reception of pure shear horizontal waves by using face-shear d24 mode piezoelectric wafers." *Smart Materials and Structures* 25.11 (2016): 11LT01.
34. Mills-Dadson, Bonaventure, et al., "Acoustic emission from damage mechanisms in composites," Structural Health Monitoring 2015, Proceedings of the Workshop on Structural Health Monitoring, Stanford University, 2015.
35. Mindlin, R. D., 1958, "Waves and Vibrations in Isotropic, Elastic Plates," Structural Mechanics, Proc Symposium on Naval Structural Mechanics, pp. 199–232.
36. Mizutani, Y., et al., "Fracture mechanism characterization of cross-ply carbon-fiber composites using acoustic emission analysis," *NDT & E International*, 2000. 33(2): p. 101-110.
37. Na, Wonjin, Dongil Kwon, and Woong-Ryeol Yu. "X-ray computed tomography observation of multiple fiber fracture in unidirectional CFRP under tensile loading." *Composite Structures* 188 (2018): 39-47.
38. Nkrumah, F., M.J. Sundaresan, and L. Uitenham. "Life prediction and life extension of composite specimens using acoustic emission technique," *Smart Structures and Materials*. 2005. International Society for Optics and Photonics.
39. Ochôa, Pedro, et al. "Detection of multiple low-energy impact damage in composite plates using Lamb wave techniques." *Composites Part B: Engineering* 80 (2015): 291-298.
40. Prosser, W. H., Michael D. Seale, and Barry T. Smith. "Time-frequency analysis of the dispersion of Lamb modes." *The Journal of the Acoustical Society of America* 105.5 (1999): 2669-2676.

41. R.D. Mindlin, J. Yang, *An Introduction to the Mathematical Theory of Vibrations of Elastic Plates*, World Scientific, Singapore, 2006.
42. Rajendra, D., A. Esterline, and Mannur Sundaresan. "A physically based classification approach for identifying AE source mechanism." *Smart Sensor Phenomena, Technology, Networks, and Systems 2010*. Vol. 7648. International Society for Optics and Photonics, 2010.
43. Reifsnider, K. and R. Jamison, "Fracture of fatigue-loaded composite laminates," *International Journal of Fatigue*, 1982. 4(4): p. 187-197.
44. Reifsnider, K.L. and S.W. Case. 2002. *Damage tolerance and durability of material systems*, Wiley-VCH.
45. Rose, J. L., 1999, *Ultrasonic Waves in Solid Media*, Cambridge University Press.
46. Rosini, Sebastian, et al. "In situ statistical measurement of local morphology in carbon-epoxy composites using synchrotron X-ray computed tomography." *Composites Part A: Applied Science and Manufacturing* 125 (2019): 105543.
47. Saeedifar, Milad, et al. "Barely visible impact damage assessment in laminated composites using acoustic emission." *Composites Part B: Engineering* 152 (2018): 180-192.
48. Sause, Markus GR, and Stefan Richler. "Finite element modelling of cracks as acoustic emission sources." *Journal of non-destructive evaluation* 34.1 (2015): 4.
49. Scholey, Jonathan J., et al. "Quantitative experimental measurements of matrix cracking and delamination using acoustic emission." *Composites Part A: Applied Science and Manufacturing* 41.5 (2010): 612-623.

50. Scott, A. E., et al. "In situ fibre fracture measurement in carbon–epoxy laminates using high resolution computed tomography." *Composites Science and Technology* 71.12 (2011): 1471-1477.
51. Scott, A. E., et al. "Influence of voids on damage mechanisms in carbon/epoxy composites determined via high resolution computed tomography." *Composites Science and Technology* 90 (2014): 147-153.
52. Sundaresan, M. J., E. G. Henneke, and K. L. Reifsnider. "Prediction of fatigue life of composite femoral prostheses using acoustic emission technique." *Journal of Composites, Technology and Research* 16.2 (1994): 127-137.
53. Sundaresan, Mannur J., and Wesley B. Williams. "Structural health monitoring of shear waves in aluminum plates." *Smart Sensor Phenomena, Technology, Networks, and Systems* 2011. Vol. 7982. International Society for Optics and Photonics, 2011.
54. Supria, Craig, "Shear Horizontal Component of Crack Growth Related Acoustic Emission Signals," MS Thesis, Mechanical Engineering, North Carolina A&T State University, 2012.
55. Tabiei, Ala, and Wenlong Zhang. "Composite laminate delamination simulation and experiment: A review of recent development." *Applied Mechanics Reviews* 70.3 (2018): 030801.
56. Takeda, Nobuo, and Shinji Ogihara. "Initiation and growth of delamination from the tips of transverse cracks in CFRP cross-ply laminates." *Composites science and technology* 52.3 (1994): 309-318.
57. Talreja, Ramesh, and Chandra Veer Singh. *Damage and failure of composite materials*. Cambridge University Press, 2012.

58. Tran, Duy. Measurement of Lamb wave Attenuation coefficients in Composite Laminates. Diss. North Carolina Agricultural and Technical State University, 2015.
59. W. Prosser, *The Propagation Characteristics of the Plate Modes of Acoustic Emission Waves in Thin Aluminum Plates and Thin Graphite / Epoxy Composite Plates and Tubes*, in: Materials Science and Engineering Department, The Johns Hopkins University, Baltimore, Maryland, 1991.
60. W.H. Prosser, M.A. Hamstad, J. Gary, A.O. Gallagher, *Finite Element and Plate Theory Modeling of Acoustic Emission Waveforms*, 18 (1999).
61. W.H. Prosser, M.R. Gorman, Plate mode velocities in graphite/epoxy plates, *Journal of Acoustical Society of America*, 96 (1994) 902-907.
62. Wang, Shi-Xun, Lin-Zhi Wu, and Li Ma. "Low-velocity impact and residual tensile strength analysis to carbon fiber composite laminates." *Materials & Design* 31.1 (2010): 118-125.
63. Whitlow, T.L., "Damage Detection and Analysis in CFRPs Using Acoustic Emission Technique," Doctoral dissertation, North Carolina A&T State University, 2013.